Carter-Penrose diagrams for emergent spacetime in axisymmetrically accreting black hole systems

Susovan Maity,[1,2,*] Md Arif Shaikh,[3,†] Pratik Tarafdar,[4,‡] and Tapas Kumar Das[1,2,§]

[1]*Department of Physics, Harish-Chandra Research Institute, Chhatnag Road, Jhunsi, Allahabad 211 019, India*

[2]*Homi Bhabha National Institute, Training School Complex, Anushakti Nagar, Mumbai 400094, Maharashtra, India*

[3]*International Centre for Theoretical Sciences, Tata Institute of Fundamental Research, Bangalore 560089, India*

[4]*The Institute of Mathematical Sciences, IV Cross Road, CIT Campus, Taramani, Chennai 600113, India*

(Received 22 May 2022; accepted 9 August 2022; published 29 August 2022)

In this work, we construct and study the Carter-Penrose diagram for sonic black hole and white hole analogs as manifested in the analog spacetime embedded inside the flow of hydrodynamic inviscid matter onto astrophysical rotating black holes. For general relativistic black hole accretion in the Kerr metric, we show that linear perturbation of the axially symmetric matter flow having certain geometrical configurations leads to the emergence of black-hole-like acoustic spacetime. Such an analog spacetime is shown to be endowed with one white-hole-like sonic horizon flanked by two black-hole-like acoustic horizons. We construct the compactified causal structures, i.e., the Carter Penrose diagrams for such emergent spacetime to study the corresponding horizon effects. For the first time in literature, the Carter-Penrose formalism is carried out for analog spacetime embedded within a natural large scale fluid flow under the influence of strong gravity.

DOI: 10.1103/PhysRevD.106.044062

I. INTRODUCTION

In this work, the Carter-Penrose diagram is used to study the properties of the sonic black hole and white hole horizons, respectively, for the emergent spacetime embedded inside the axially symmetric flow of hydrodynamic accretion onto astrophysical black holes. Low angular momentum axisymmetric black hole accretion in the Kerr metric may manifest multitransonic behavior. In order to pass through more than one sonic point, accretion solutions must undergo a shock transition [1–24]. For such shocked accretion, subsonic flow of hydrodynamic matter starting from a large distance becomes supersonic after crossing a sonic point located at a relatively large distance from the black hole horizon. Such supersonic flow may then encounter a discontinuous stationary shock and becomes subsonic again. Shock induced subsonic flow then passes through another sonic point located at the close proximity of the horizon. A shocked multitransonic accretion flow, thus, connects four different regions consisting of two subsonic regions and two supersonic regions from infinity to the innermost radius up to which the flow solutions can be extended.

Transonic accretion onto a black hole can be posed as a two-dimensional dynamical system problem as defined in dynamical systems theory. Using the structure of dynamical systems, it is possible to show that a stationary transonic black hole accretion solution may be realized as a critical solution on a phase portrait characterized by the flow Mach number M (defined by the ratio of the dynamical flow velocity and the characteristic sound speed) and the radial distance r from the black hole horizon measured along the equatorial plane of the flow [25–35]. A multitransonic flow resembles a multicritical phase orbit passing through two out of three critical points, where the two are saddle type critical points and the third one is a center type critical point located in between aforementioned saddle points.

Whether any one-to-one mapping between a critical point in the $M - r$ phase portrait and the corresponding sonic point of the flow exists will actually depend on the geometrical configuration of the accretion flow. Axially symmetric hydrodynamic accretion in the Kerr metric may, in principle, be studied for the following three different geometric configurations of the flow [36–39]:

(i) Flow with constant thickness, where the flow thickness will not vary with the radial distance as

*susovanmaity@hri.res.in
†arif.shaikh@icts.res.in
‡pratikt@imsc.res.in
§tapas@hri.res.in

measured along the equatorial plane of the disc. For any such flow considered in this paper, corresponding flow variables will be characterized by a subscript CH.

(ii) Conical flow, for which the flow thickness is proportional to the radial distance r, i.e., the ratio of the flow thickness and the radial distance is constant for all values of r. The flow geometry is then characterized by the solid angle Θ subtended by the disc at the horizon. This configuration is supposed to be the most ideal one to portray a low angular momentum inviscid disc. For any such conical flow considered in this paper, corresponding flow variables will be characterized by a subscript CF.

(iii) Flow in hydrostatic equilibrium along the vertical or the transverse (perpendicular to the equatorial plane) direction, for which the flow thickness is found to be a nonlinear function of the local radial distance. The expression for such flow thickness contains the expression of the characteristic radial sound speed, although the Euler equation is not formulated and solved along the vertical direction. For such flows considered in this paper, we will only use a model prescribed by Novikov-Thorne which will be described later. Thus corresponding flow variables will be characterized by a subscript NT.

It has been observed that for general relativistic accretion flow in the Kerr metric with constant height flow as well as with conical flow, the critical points in the phase portrait and the corresponding sonic points coincide, i.e., the value of the Mach number becomes unity at the critical points. For flow in hydrostatic equilibrium along the transverse direction, however, the Mach number becomes less than unity at the critical point for adiabatic equation of state of the accreting fluid. Hence, for the stationary definition of characteristic sound speed $c_s = \sqrt{\gamma p/\rho}$, the sonic point forms at a distance smaller compared to the location of the critical point, where γ is the ratio of the specific heats at constant pressure and at constant volume, respectively ($\gamma = c_p/c_v$), p and ρ being the pressure and the mass density of accreting fluid.

The nonisomorphism between the critical and the sonic points for flow in hydrostatic equilibrium along the transverse direction can be approached in two different ways. In a conventional approach, one considers the expression of the characteristic sound speed, following the stationary definition of the same, and numerically integrates the flow equation inward (toward the black hole event horizon), starting from the critical point (using the critical point conditions) up to the radial distance where the stationary Mach number becomes unity and designates that radial location to be the location of the sonic point (see, e.g., [15] for the detailed description of how one can locate the sonic point by numerically integrating the corresponding flow equations). Very recently, in an alternative approach, the dynamical definition of the sound speed has been found for general relativistic accretion onto Schwarzschild black holes, by perturbing the flow equations using a spacetime-dependent stability analysis. The expression of such effective sound speed differs from the stationary definition of c_s and hence such dynamical sound speed has been dubbed as the "effective sound speed" $c_{\rm eff}$. If one considers the dynamically motivated effective sound speed instead of the stationary definition of sound speed, the critical and the sonic points coincide, and this isomorphism due to redefinition of sound speed is evident even from the stationary analysis of the accretion itself (see, e.g., [24] for further details).

Accreting black hole systems are quite versatile to study in the sense that not only are such systems investigated from the context of astrophysics as well as of the dynamical systems theory, but also such systems can be considered as a realistic example of classical analog gravity models. The analog gravity phenomena is realized by linearly perturbing a transonic fluid where a black-hole-like analog spacetime structure with acoustic horizons emerges, where such analog spacetime structure has a unique correspondence with a particular transonic flow line of the fluid considered [40–43]. It has been established that by linearly perturbing the transonic accretion flow, a black-hole-like emergent acoustic spacetime can be produced within the accreting fluid [17,37,44–54]. An accreting black hole system is considered a unique example of a classical analog gravity model since both kinds of horizons, the analog (acoustic, or sonic) as well as the gravitational one, are present in the same system. The sonic points have usually been identified with acoustic horizons, and for multitransonic shocked accretion, the corresponding sonic geometry contains two black-hole-type acoustic horizons (which actually are two sonic points of the flow) and a white-hole-type acoustic horizon formed at the stationary shock location.

For constant height flow as well as for conical flow, the critical points are designated as the location of the acoustic horizons, since the critical points and the sonic points coincide for these flow geometries. For accretion in hydrostatic equilibrium along the transverse direction, however, there are ambiguities in determining the location of the acoustic horizons. If one considers the stationary definition of sound speed, then the sonic points are the acoustic horizons and not the critical points. On the other hand, if we chose the dynamical effective sound speed to be the speed of propagation of the acoustic perturbation traveling inside the linearly perturbed accretion flow, then the critical point itself becomes the sonic point and hence the acoustic horizons are supposed to form at the critical point. It is, however, to be noted that the definition of effective sound speed is essentially local, i.e., the expression of such dynamical sound speed is defined based on its behavior only at the corresponding critical points and such $c_{\rm eff}$ can

only be defined globally, on every radial point, by analytical continuation imposed by the global redefinition. One thus needs to introduce a more concrete scheme for identifying the exact location of the acoustic horizon for analog spacetime associated with accreting black hole systems, as well as to understand the global structure of such nontrivial emergent spacetime.

The most common approach to the problem of analyzing the global structure of spacetime consisting black holes and white holes, in the context of classical gravity, is to find a Kruskal-like diagram for the corresponding spacetime metric. The coordinate transformations needed to write down the Kruskal-like metric generally involves analytical continuation, i.e., the spacetime manifold represented by the complete range of the original coordinates becomes a subset of the spacetime manifold represented by the new Kruskal-like coordinates. The uniformity and simple orientation of light cones make a Kruskal-like diagram a very suitable candidate for analyzing the global causal structure of such spacetime. But even in the context of classical general relativity, a spacetime consisting of black holes and white holes can be specified by a small number of parameters, thus making the spacetime still much simpler than that which is created by a compact object.

Thus for this kind of simplistic spacetime one may consider the possibility of further analytical continuation, such that, the Kruskal-like spacetime becomes a subset of a much more general manifold. In order to explore the possibility one must compactify the infinities of the Kruskal-like coordinates into a finite region. For example, just the introduction of a spin parameter in a black hole spacetime gives way to a rotating black hole spacetime, which can be described by the Kerr metric. The Kruskal-like diagram is obviously more interesting than Schwarzchild black holes, as the rotation of a black hole becomes responsible for degenerate horizons. But compactifying the Kruskal-like diagram for the Kerr metric and further analytical continuation gives rise to a much richer global structure involving infinite numbers of black holes and white holes in multiple universes connected in a specific geometrical way. The best tool for the visualization and interpretation for this kind of compactification is the Penrose-Carter diagram [55–59], not only for the Kerr or other kind of black hole spacetimes, but also for cosmological spacetimes.

Motivated by the aforementioned discussions, in the present work we propose that construction of a Carter-Penrose diagram will unambiguously identify the corresponding sonic horizons for accreting black hole systems, irrespective of the geometrical configuration of the flow. Furthermore, the novelty of the approach lies in the fact that the numerical construction scheme for a Carter-Penrose diagram can be applied to any generic fluid configuration which is not necessarily a fluid system accreting onto a black hole. The same numerical method used to construct the Carter-Penrose diagrams for accreting fluid thus can be used to probe the causal nature of any kind of stationary fluid solutions, which may be that associated with usual condensed matter systems typically used to probe into the nature of Hawking radiationlike effect from the acoustic horizons. The condition for the flow to be stationary is satisfied by a number of analog systems including the condensed matter example mentioned above. Another advantage of the method used is that once the transformations necessary to construct the Carter-Penrose diagram for different patches of the whole analog spacetime corresponding to any stationary flow for any analog system is specified, the numerical scheme automatically takes care of the orientation of the patches stacked together, although once the orientation of the diagram is understood from the initial plots of the diagram, one has to manually take care of the displacement of the patches as the inverse trigonometric functions involved in the transformations are inherently single valued functions, which superposes one patch on another if displacement is not manually put. The scheme to plot the Carter-Penrose diagrams is also capable of taking care of any discontinuous jump between one subsonic and another supersonic region, which occurs in any stationary fluid flow as it continuously connects the two patches on the two sides of the discontinuity, an interesting feature that can be extracted about the discontinuous sonic barrier.

In this work we use one model each from two different kinds of flows as previously mentioned. We first choose the accretion flow with certain geometry for which the critical points are the same as the sonic points. In this aspect the constant height flow and the conical flows are equivalent. We consider the conical flow since it portrays low angular momentum flow better in comparison to the constant height flow. We then find the critical points as well as the critical point conditions, and construct the corresponding phase portraits for such a flow. Then we linearly perturb the flow to obtain the analog spacetime (thus the corresponding analog metric) and construct the Carter-Penrose diagram using the metric elements of the acoustic metric to identify the acoustic black hole horizons at the critical points and the acoustic white hole horizon at the shock location. We perform such calculations for both adiabatic as well as for the isothermal flow.

The other kind of accretion flow that we consider is accretion in hydrostatic equilibrium along the transverse direction for functional form of the local disc heights as introduced by Novikov and Thorne [60] and mention the fact that the local disc height by Riffert and Herold [61] will have a similar treatment for reasons that will be clarified in subsequent sections. We perform the critical point analysis to find out the critical point conditions and show that the critical points are not the same as sonic points if one considers the stationary sound speed. We construct the corresponding phase portrait to identify the sonic points and the shock locations for the multitransonic shocked

flow. We then perturb the flow equations to construct the relativistic acoustic geometry and find out the expression for the effective sound speed as defined at the corresponding critical points. Finally we construct the corresponding Carter-Penrose diagram and establish that the acoustic horizons are formally located at the critical point of accretion flow in hydrostatic equilibrium along the vertical direction if one considers the dynamical definition of the effective sound speed. Since a Carter-Penrose diagram can formally identify the location of the horizons, we ensure that the dynamical definition of effective sound speed is an important quantity when the critical points and the sonic points (sonic points defined in terms of the stationary sound speed) do not coincide for accretion onto a rotating black hole.

For the first time in literature, the Carter-Penrose diagram has been constructed and used to study the analog geometry embedded in transonic fluid for any real physical system whose fluid properties are dependent on underlying physics. We thus use the Carter-Penrose diagram to study the emergent spacetime embedded inside transonic accretion onto Kerr black holes.

II. GOVERNING EQUATIONS FOR POLYTROPIC FLOW AND CHOICE OF THE FLOW THICKNESS

We consider low angular momentum, inviscid, axially symmetric, irrotational accretion flow around a Kerr black hole for two different geometric configurations of the flow. The background metric and fluid equations are the same for both of the flow geometries we are considering. The difference arises from the height prescriptions we consider where one disc has a conical cross section, i.e., the height linearly rises with the radial distance and the other one is in hydrostatic equilibrium. Below the details of the models are specified. Then critical point analysis and causal structure analysis of emergent acoustic metrics are performed. In this work we will be working in the natural units of $G = 1$, $c = 1$, $M = 1$ for convenience, where G stands for the gravitational constant, c is the speed of light, and M stands for the mass of the black hole in consideration.

A. Background metric of a Kerr black hole

The background spacetime metric, as proposed by Boyer and Lindquist [58] at its equatorial plane, can be expressed in terms of cylindrical coordinates and using the method of vertical averaging as described in [62]; it can be written as

$$ds^2 = -\frac{r^2\Delta}{A}dt^2 + \frac{r^2}{\Delta}dr^2 + \frac{A}{r^2}(d\phi - \omega dt)^2 + dz^2, \quad (1)$$

where

$$\Delta = r^2 - 2r + a^2, \quad A = r^2 + r^2a^2 + 2ra^2, \quad \omega = \frac{2ar}{A}. \quad (2)$$

Here $a = J/M$ is the Kerr parameter, where J and M represent the total angular momentum and the total mass of the rotating black hole, respectively.

In order to analyze the dynamics of the accretion disc outside the black hole, we must specify the horizon of the background metric corresponding to the Kerr black hole, r_+, given by

$$r_+ = 1 + \sqrt{1 - a^2}. \quad (3)$$

B. The Euler equation, continuity equation, and the equation of state

The energy-momentum tensor for a perfect fluid is given by

$$T^{\mu\nu} = (p + \epsilon)v^\mu v^\nu + pg^{\mu\nu}, \quad (4)$$

where ρ is the rest-mass energy density of the fluid, so that $\epsilon = \rho + \epsilon_{\text{thermal}}$, and p is the pressure of the fluid. v^μ is the four-velocity with the normalization condition $v^\mu v_\mu = -1$.

In the cylindrical Boyer-Lindquist frame, which is our choice for the coordinate system, the four velocity components can be expressed in terms of the advective velocity u, which is the three-component velocity in the corotating frame [63]. Now, the temporal component of four-velocity v_t in terms of u is given by

$$v_t = \sqrt{\frac{\Delta}{B(1 - u^2)}} \quad (5)$$

where $B = g_{\phi\phi} + 2\lambda g_{t\phi} - \lambda^2 g_{tt}$ and the specific angular momentum λ is given by $\lambda = -v_\phi/v_t$. The radial component of the four-velocity v^r in terms of u is given by

$$v^r = \frac{u\sqrt{\Delta}}{r\sqrt{1 - u^2}}. \quad (6)$$

The fluid equations cannot be analytically integrated if a barotropic fluid equation is considered. We first demonstrate the entire work for polytropic accretion and then summarize the entire work for isothermal accretion where complexities regarding nonisomorphism of critical and sonic points do not arise. The equation of state for adiabatic flow is given by $p = k\rho^\gamma$ where γ is the polytropic index and k is constant. The sound speed for adiabatic flow (isoentropic flow) is given by

$$c_s^2 = \left.\frac{\partial p}{\partial \epsilon}\right|_{\text{entropy}} = \frac{\rho}{h}\frac{\partial h}{\partial \rho}, \quad (7)$$

where h is the enthalpy given by

$$h = \frac{p+\varepsilon}{\rho}. \tag{8}$$

The continuity equation and the Euler equation are given by, respectively,

$$\nabla_\mu(\rho v^\mu) = 0 \tag{9}$$

and

$$\nabla_\mu T^{\mu\nu} = 0. \tag{10}$$

For adiabatic flow, the Euler equation simplifies as

$$v^\mu \nabla_\mu v^\nu + \frac{c_s^2}{\rho}(v^\mu v^\nu + g^{\mu\nu})\partial_\mu \rho = 0 \tag{11}$$

where expression of c_s^2 is given by Eq. (7).

C. Choice of disc heights

As mentioned in Sec. I, simplistic accretion disc structure like a conical disc, where $H(r)$ is a linear function of radial distance, has the property that the critical point turns out to be also the point where advective velocity is equal to the sound speed. Thus the critical points in this model turn out to be the sonic points also. An accretion disc with constant height also has the same property. But we will only consider conical flow as the representative of this kind of model with isomorphic critical points and sonic points as it portrays low angular moment accretion most accurately. The height of a conical disc as a function of radial distance is given by

$$H_{CF}(r) = \Theta r \tag{12}$$

where, as previously mentioned, Θ is the angular span of the conical structure.

There are three prescriptions for the height function in hydrostatic equilibrium, for none of which the critical points and sonic points coincide. The oldest, and most used expression for the disc thickness for accretion flow maintained in the hydrostatic equilibrium along the vertical direction, was provided by Novikov and Thorne [60] as

$$H_{\rm NT}(r) = \left(\frac{p}{\rho}\right)^{\frac{1}{2}} \frac{r^3 + a^2 r + 2a^2}{r^{\frac{3}{2}} + a} \sqrt{\frac{r^6 - 3r^5 + 2ar^{\frac{9}{2}}}{(r^2 - 2r + a^2)(r^4 + 4a^2r^2 - 4a^2 r + 3a^4)}}. \tag{13}$$

It is to be noted that accretion flow described by the above disc thickness cannot be extended up to r_+. The flow will be truncated at a distance r_T, where

$$(r_T)^{\frac{1}{2}}(r_T - 3) = 2a \tag{14}$$

which is outside r_+. In reality of course the flow will exist up to r_+ but no stationary integral flow solutions can be constructed up to the close proximity of r_+ for accretion flow described by the disc height prescribed by Novikov and Thorne.

Riffert and Herold [61] provided an expression of disc thickness by modifying the gravity-pressure balance condition of the treatment done in Novikov and Thorne. In the work of Novikov and Thorne, the vertical component of gravity was replaced by zR^z_{0z0} in the vertical component of the Newtonian gravity pressure balance equation. Riffert and Herold on the other hand used the Euler equation directly to find out the gravity pressure balance equation and the height expression as formulated by them is given by

$$H_{\rm RH}(r) = \left(\frac{p}{\rho}\right)^{\frac{1}{2}} \sqrt{\frac{r^5 - 3r^4 + 2ar^{\frac{7}{2}}}{r^2 - 4ar^{\frac{1}{2}} + 3ar^2}}. \tag{15}$$

In this case also the flow can only be extended up to r_T as given by (14). We see that both of the disc heights can be expressed in the form by $H(r) = (p/\rho)^{1/2} f(r, a)$. The prefactor in this expression is related to sound speed and thus these two height expressions are dependent on the flow variable itself. As will be seen later, this particular form of both of the disc heights given by Eqs. (13) and (15) is responsible for the fact that critical points do not coincide with the transonic points. This particular general form of the height expression for both of these models is responsible for the fact that they also have the same Mach number at the critical points. Thus choosing any one of these models will be sufficient to demonstrate this kind of nonisomorphism of critical points and sonic points.

More recently Abramowicz, Lanza, and Percival [64] introduced an expression for the disc thickness, given by

$$H_{\rm ALP}(r) = \left(\frac{p}{\rho}\right)^{\frac{1}{2}} \sqrt{\frac{2r^4}{v_\phi^2 - a^2(v_t - 1)}}, \tag{16}$$

where v_ϕ and v_t are the azimuthal and time component of the four-velocity of accreting fluid.For this height function, the steady state accretion solutions can be obtained up o r_+. It is, however, to be noted that by linearly perturbing the flow equation for flow thickness (16), the acoustic metric could not be constructed as of now. Thus we will not be using this height expression for stationary analysis as it

cannot be used for later analysis involving an acoustic metric.

In our present work, we thus use the height function due to Novikov and Thorne only as a representative of models where critical points are not transonic points.

Although the complete specification of the accretion model we will be working with has been presented, we must clarify that, certain terminology regarding the velocities and other quantities defined above will be used throughout this work. The reason is that, a perturbation analysis will be used to study dynamics of first order perturbations, which will be performed on steady state flow. Thus we must use a nomenclature to distinguish between the steady state and first order flow. We will frequently denote v_0^μ, u_0 as four-velocity and advective velocity corresponding to the steady state flow. In general, we will use the subscript zero to denote the value of any physical variable corresponding to the stationary solutions of the steady flow, e.g., p_0, ρ_0 etc. We will define the first order perturbation of any physical variable to have a subscript of one where the perturbation analysis will be carried out. No use of subscript on any variable in some equation denotes that the equation is valid in the dynamical case and the variable is the sum of the steady state part and the dynamical first order part.

III. DESCRIPTION OF MULTITRANSONIC ADIABATIC FLOW AS A DYNAMICAL SYSTEM PROBLEM

In order to represent the problem of stationary accretion of an ideal fluid following adiabatic equation of state around a rotating black hole, one must find the specific form of the governing fluid equations as specified in Eqs. (9) and (11) for the two height functions as specified in Eqs. (12) and (13). It will be shown in this section that solving the problem of stationary accretion, i,e., describing the dynamics of a compressible astrophysical fluid essentially boils down to solving a set of differential equations involving the derivative of advective velocity du_0/dr and derivative of dc_{s_0}. The problem can also be dealt with by solving one differential equation involving the expression of du_0/dr and an algebraic equation simultaneously. This later approach will be followed in this work. Thus the plan of work in this section will be as follows.

We will first integrate the general forms of the dynamical equation and obtain two integrals of motion as one of the expressions involving the specific energy, denoted by $\mathcal{E}_0$, will be used as the aforementioned algebraic equation. Next we derive the specific form of the derivative of advective velocity du_0/dr. Here we will see how the analytical structure of an accreting fluid system can be formulated as a problem of a dynamical system. The initial condition relating sound speed and advective velocity of the fluid at the critical points will also be derived for both kinds of accretion flows having a conical disc height and disc height as proposed by Novikov and Thorne. From the critical conditions, the isomorphism of critical and sonic points for accretion flow with conical disc and nonisomorphism of critical and sonic points for accretion flow with disc height as proposed by Novikov and Thorne will be pointed out. In the next part it will be demonstrated how multitransonic solutions of the accretion can be constructed from critical solutions of the dynamical system of equations for a specific subset of the parameters of the problem. Once one obtains the multitransonic solution, the flow line is determined and we will proceed for the perturbation analysis in the next section.

A. The first integrals of motion

In order to establish the problem of accretion as a dynamical system, two first integrals of motion for the stationary flow are needed. We first deal with the Euler equation as the height function does not enter in the equation. Then we differentiate between the conical flow and Novikov-Thorne type disc when we deal with the continuity equation.

The conservation of the temporal component of the simplified version of the Euler equation given by Eq. (11) leads to the constancy of specific energy of the accreting fluid $\mathcal{E}_0$, given by

$$\mathcal{E}_0 = \frac{\gamma - 1}{\gamma - 1 - c_{s0}^2}\sqrt{\frac{\Delta}{B(1-u_0^2)}}. \tag{17}$$

The second integral of motion obtained by integrating the continuity equation is the mass accretion rate $\dot{M}$, although we will later use Ψ instead of $\dot{M}$ for simplification of notation. $\dot{M}$ can be expressed as

$$\dot{M} = 4\pi H(r) r \rho \frac{\sqrt{\Delta} u_0}{r\sqrt{1-u_0^2}}. \tag{18}$$

The entropy accretion rate $\dot{\Xi}$ is proportional to $\dot{M}$ and can be expressed as

$$\dot{\Xi} = \left(\frac{1}{\gamma}\right)^{\left(\frac{1}{\gamma-1}\right)} 4\pi \Delta^{\frac{1}{2}} c_s^{\left(\frac{2}{\gamma-1}\right)} \frac{u}{\sqrt{1-u^2}} \left[\frac{(\gamma-1)}{\gamma-(1+c_s^2)}\right]^{\left(\frac{1}{\gamma-1}\right)} H(r). \tag{19}$$

We thus have two primary first integrals of motion along the streamline—the specific energy of the flow $\mathcal{E}$ and the mass accretion rate $\dot{M}$. Even in the absence of creation or annihilation of matter, the entropy accretion rate $\dot{\Xi}$ is not a generic first integral of motion. As the expression for $\dot{\Xi}$ contains the quantity $K \equiv p/\rho^\gamma$, which is a measure of the specific entropy of the flow, the entropy accretion rate $\dot{\Xi}$ remains constant throughout the flow only if the entropy per particle remains locally invariant. This condition may

be violated if the accretion is accompanied by a shock and as we will see in the next section, the multitransonic solution will have a shock present in the flow line. However, $\dot{\Xi}$ is an important quantity needed to distinguish between flows having different topological structure in phase portraits for different values of parameters. We do not study the parametric variation of flows as we only focus on accretion flow where shock will be present. Still, $\dot{\Xi}$ is required in order to find the expression of du_0/dr.

B. Velocity gradient and derivation of critical conditions

One obtains two linear equations involving the derivative of the advective velocity du_0/dr and the derivative of sound speed dc_{s0}/dr by taking derivatives of the two constants of integration. If the expression of dc_{s0}/dr from one equation is substituted in the other equation, then one gets the expression of the derivative of advective velocity. While taking the derivative of Eq. (19) the two height expressions given by Eqs. (12) and (13) are used separately.

The expression for the derivative of advective velocity u_0 corresponding to the flow with conical height function turns out to be (see [62])

$$\left.\frac{du_0}{dr}\right|_{CF} = \frac{u_0(1-u_0^2)[c_{s0}^2\frac{2r^2-3r+a^2}{\Delta r}+\frac{1}{2}(\frac{B'}{B}-\frac{\Delta'}{\Delta})]}{u_0^2-c_{s0^2}} = \frac{N_{CF}}{D_{CF}}. \tag{20}$$

The expression for the derivative of advective velocity u_0 corresponding to the flow with height function as prescribed by Novikov and Thorne turns out to be (see [24])

$$\left.\frac{du_0}{dr}\right|_{\mathrm{NT}} = \frac{u_0(1-u_0^2)[\frac{2}{\gamma+1}c_{s0}^2(\frac{\Delta'}{2\Delta}+\frac{f'}{f})+\frac{1}{2}(\frac{B'}{B}-\frac{\Delta'}{\Delta})]}{u_0^2-\frac{c_{s0^2}}{(\frac{\gamma+1}{2})}} = \frac{N_{NT}}{D_{NT}}. \tag{21}$$

In both equations mentioned above, the numerator is denoted as N and the denominator as D. One can thus define some parameter τ such that $du_0/d\tau = N$, $dr/d\tau = D$. In this way the problem of finding all the time-independent fluid profile of accretion can be posed as a problem of dynamical systems. Now we will use the tools of nonlinear dynamics to find the critical points and then later to draw the critical flows in phase portraits.

The critical points can be obtained by setting $du_0/d\tau = 0, dr/d\tau = 0$ simultaneously. Thus the critical point conditions turn out to be $N = 0$ and $D = 0$.

Thus for conical flow, the condition $D = 0$ at the critical point yields

$$u_0^2|_{r=r_c} = c_{s0}^2|_{r=r_c} \tag{22}$$

whereas for flow with height function as prescribed by Novikov and Thorne, the condition $D = 0$ turns out to be

$$u_0^2|_{r=r_c} = \frac{c_{s0}^2|_{r=r_c}}{(\frac{\gamma+1}{2})} \tag{23}$$

or for later convenience we can write

$$u_0^2|_{r=r_c} = \frac{c_{s0}^2|_{r=r_c}}{1+\beta}, \quad \text{where } \beta = \frac{\gamma-1}{2}. \tag{24}$$

The key point we get from Eqs. (22) and (23) is that the Mach number, i.e., the ratio of advective velocity and sound speed, is 1 at the critical point for conical flow. But for disc height as prescribed by Novikov and Thorne, the Mach number is $\sqrt{1/1+\beta}$ at critical points, which is always less than unity for $\gamma > 1$. Thus the critical points and the sonic points are isomorphic in the case of conical flow, but for disc height described by Novikov and Thorne, the sonic and critical points are not isomorphic.

The value of sound speed at critical points can be obtained from the other critical condition $N = 0$ and by substituting the value of sound speed and corresponding value of advective velocity in Eq. (17), one obtains the radii of the critical points. The value of the derivative of the advective velocity at the critical points can also be obtained and thus along with the locations of the critical points, the complete set of initial conditions needed to integrate Eqs. (20) and (21) are obtained. At this point one needs to specify the parameters of the problem so that the phase portraits can be plotted by solving the expressions for the derivatives of advective velocity.

C. Nature of critical points and phase portrait for multitransonic accretion

The detailed method of obtaining a multitransonic flow line in the phase portrait from the initial critical conditions corresponding to conical flow has been described in [51] and the same method for disc height as prescribed by Novikov and Thorne has been described in [24]. But in order to perform perturbation analysis on a certain flow line, we must first describe the nature of the critical points and the solutions passing through them, namely the critical flow lines. Finally we choose a particular flow line consisting of the critical flow lines such that multitransonicity is achieved.

To numerically obtain phase portraits, Eqs. (20) and (21) have to be integrated and one needs to specify the parameters needed to solve this problem which are present in the equations and in the initial conditions. There are four parameters given by $\mathcal{E}_0$, λ, γ, and a for both kinds of flows with the conical height function and the height function as prescribed by Novikov and Thorne. The topology of the flow is dependent on the values of parameters.

As previously mentioned, we want to focus on the characteristics of multitransonic accretion in this work. For the dynamical system corresponding to the models of accretion we are concerned with, there exists only one sonic point corresponding to each saddle type critical point. A physically acceptable transonic solution can be constructed only through a saddle type critical point, and not through a center type critical point. Hence the concept of a sonic point corresponding to a center type critical point is meaningless. Thus in order to choose a multitransonic accretion flow, we must choose the parameters such that the dynamical system corresponding to the flow has multiple critical points and the critical flows correspond to accretion and not wind.

The numerical plots of the critical flows in the phase portraits for both kinds of flows with conical height function and height function as prescribed by Novikov and Thorne are presented in Fig. 1, such that the chosen parameters correspond to multicritical accretion for both flows.

In both figures portrayed in Fig. 1, $r_{\rm out}$ and $r_{\rm in}$ correspond to the outer and inner critical points, respectively, both of which are saddle type critical points. The critical point which resides in the middle of the outermost critical point located at $r_{\rm out}$ and innermost critical point $r_{\rm in}$ is center type in nature, although not shown explicitly in the plot of critical flow lines as the point plays no role in a multitransonic flow line.

In Fig. 1, the parameters of the problems are chosen such that the phase portrait corresponds to accretion flow with multiple critical points. But the presence of multiple critical points does not itself ensure the presence of multitransonic flow. From the figures it is clear that a continuous critical flow through either of the two saddle type critical points in the phase portrait will not pass through the other saddle type critical point. One can only choose a multitransonic flow consisting of the critical solutions if there is a mechanism that allows a discontinuous jump from the supersonic critical flow line through the outer critical point $r_{\rm out}$ to the subsonic critical flow line through the innermost critical point $r_{\rm out}$. This discontinuity in an accretion flow can be physically modeled by a Rankine-Hugoniot type infinitesimally thin shock. There is a subset of parameters within the parameter space corresponding to multitransonic accretion, where shock may occur. In the plot of the critical solutions in the phase portrait, the parameters are chosen for both flows in such a way that such a shock occurs. The fluid elements in the disc accretion flows in hydrostatic equilibrium irrespective of the height function of the disc, start far away from the accretor, in this case, the black hole, along the critical flow line, and move through the outer critical point $r_{\rm out}$, continue along the flow line (the blue solid line passing through $r_{\rm out}$ in the online version of the figure), and will be supersonic till the flow variables and thermodynamic variables make a discontinuous jump to

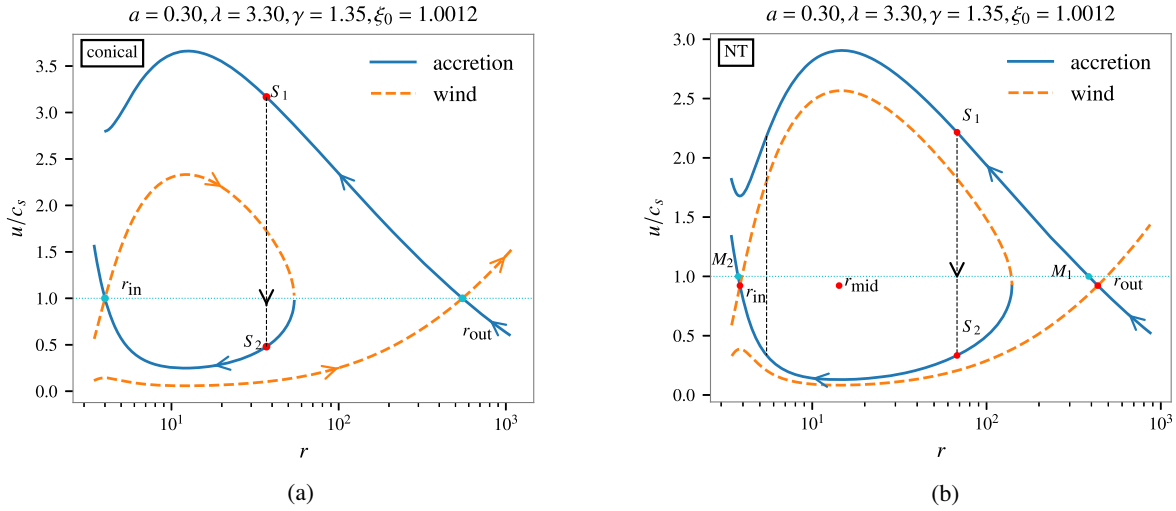

FIG. 1. (a) Phase portrait for adiabatic flow with conical disc height. (b) Phase portrait for adiabatic flow with height expression formulated by Novikov and Thorne. Both phase portraits have been drawn for adiabatic accretion with the set of parameter values $\mathcal{E}_0 = 1.0012$, $\lambda = 3.30$, and $\gamma = 1.35$. For both pictures the blue solid lines correspond to the accretion branch whereas the orange dashed lines correspond to the wind branch. The innermost critical point is denoted as $r_{\rm in}$ and outermost critical point is denoted as $r_{\rm out}$. S_1 corresponds to the point in the phase portrait in the accretion branch through the outer critical point where shock may occur and S_2 corresponds to the point where shock occurs in the accretion branch through the inner critical point. The same radial distance of S_1 and S_2 corresponds to the fact that the shock is infinitesimally thin. The dotted black line joining S_1 and S_2 corresponds to the discontinuous jump in the shock location. (b) Phase portrait of flow with height as prescribed by Novikov and Thorne; the Mach number at critical points are not unity and thus the critical point and sonic points do not coincide for this height prescription. The outer sonic point and the inner sonic point in the phase portrait corresponding to the flow with height function as prescribed by Novikov and Thorne are, respectively, M_1 and M_2.

another branch (the green dotted line in the online version of the figure) as a consequence of shock. The discontinuous jump occurs at S_1 where the flow passing through the outer critical point is supersonic and reaches S_2 on the flow line passing through the inner critical point, where the flow becomes subsonic again. Then the fluid element eventually goes through $r_{\rm in}$. This discontinuity is strictly a discontinuity of the values of the fluid variables and not a discontinuity present in the physical flow. In this way the presence of shock makes the fluid element move through a multitransonic flow line. Thus we not only choose the parameters to allow multiple critical points but also to allow multitransonic accretion.

By following the aforementioned scheme, we are able to choose a multitransonic accretion flow line for each of the flows corresponding to the conical height function and height function as prescribed by Novikov and Thorne. The major difference between the flow lines of the two models is that whereas the flow achieves transonicity at $r_{\rm out}$ and again at $r_{\rm in}$ for conical flow, the flow for disc height as prescribed by Novikov and Thorne does not, as the Mach number is less than one at $r_{\rm out}$ and $r_{\rm in}$. For flow with disc height as prescribed by Novikov and Thorne, a fluid element of the flow becomes subsonic to supersonic for the first time at M_1 and after it becomes supersonic to subsonic at the shock location, it becomes supersonic for the second time at M_2 as shown in Fig. 1(b).

Before concluding the discussions about the stationary solutions of accretion flow, we note that, we have so far established the nonhomomorphism of critical and sonic points for flow with disc height as prescribed by Novikov and Thorne. One can simply assert that the fact that the critical point and sonic point do not coincide is just a feature of the height function as prescribed by Novikov and Thorne. This feature does not necessarily make us question how correct the definition of sound speed is in a dynamical context. To answer this question one may try to perturb the dynamical equations governing the flow and try to find out how linear perturbation behaves as sound speed at its core is the speed of propagation of first order perturbation in a medium. The systematic analysis of perturbations of fluid equations leads to treating a certain linearly perturbed fluid variable from the context of analog or emergent gravity. The perturbation analysis has been performed in the next section and the connection with analog gravity is established.

IV. DERIVATION OF ACOUSTIC METRIC FROM LINEAR PERTURBATION OF FLUID EQUATIONS

The nonhomomorphism of critical points and sonic points established in the previous section does not necessitate one to redefine sound speed as the stationary picture does not suggest how the acoustic perturbation propagates in the accreting medium. The motivation of this work will thus only be clear when one performs a perturbation analysis of the full spacetime-dependent fluid equations. In this section we perturb the dynamical equations describing adiabatic accretion flow in the background metric of a rotating black hole for conical disc height as well as disc height as prescribed by Novikov and Thorne. The perturbations yield dynamical equations governing the first order perturbation of a certain flow variable. Then the acoustic metric is written by comparing the aforementioned governing equations with the equation of a massless scalar field in curved spacetime. The basic methodology of analog gravity is based on identifying the similar forms of the governing equation of first order perturbation of a certain fluid variable and the massless scalar field equation in curved spacetime. The analogy is subject to certain conditions on the flow which are already fulfilled by our choice of ideal inviscid fluid. Thus for an acoustic metric describing the perturbation in the accretion flow with height function as prescribed by Novikov and Thorne, we show that, the acoustic black hole horizons are located at the critical points. To conclude this section we define an effective sound speed, for which the sonic points turn out to be critical points.

As our work concerns two disc models, we must differentiate the two emergent metrices as well. Although that will be done by the end of this section, it must be mentioned how the differences in the functional forms of conical disc height and disc height as prescribed by Novikov and Thorne are manifested in the perturbation analysis. If we compare Eq. (12) describing the height function for conical flow and Eq. (13) describing the height function formulated by Novikov and Thorne, we see that the perturbation of flow variable will have no consequence on the perturbation of conical flow as it is only a function of radial distance and on the other hand it will be directly manifested in the perturbation of flow with disc height prescribed by Novikov and Thorne as it directly depends on the sound speed, a flow variable, in the case of adiabatic flow. Thus we will differentiate between the two models where perturbation of height is introduced in this section and the parameter distinguishing the two flows will turn out to be β as defined in Eq. (24) corresponding to only flow with height function as prescribed by Novikov and Thorne. We will use the notation β for conical flow also and fix its value to zero so that the equations describing the perturbations have the same structural form. When we write down the acoustic metric we will use β only for flows with height function as prescribed by Novikov and Thorne and remove β from the expression of acoustic metric for conical flow by setting it to zero.

Now the perturbation on the stationary flow is done by following standard linear perturbation analysis [50,52,65,66] where the acoustic spacetime metric for conical flow was derived. Time-dependent accretion variables, like the components of four-velocity and pressure are written as small time-dependent linear perturbations added to their stationary values. Thus we can write

$$v^t(r,t) = v_0^t(r) + v_1^t(r,t),$$
$$v^r(r,t) = v_0^r(r) + v_1^r(r,t),$$
$$\rho(r,t) = \rho_0(r) + \rho_1(r,t), \tag{25}$$

where the subscript 1 denotes the first order small perturbation of some variable about the stationary value denoted by subscript 0. The second constant of integration from continuity equation $\dot{\mathcal{M}}$ or Ψ has the form (see [24,62])

$$\Psi = 4\pi\sqrt{-g}\rho(r,t)v^r(r,t)H_\theta \tag{26}$$

which is the stationary mass accretion rate of the accretion flow. Thus

$$\Psi(r,t) = \Psi_0 + \Psi_1(r,t) \tag{27}$$

where Ψ_0 is the stationary mass accretion rate defined in Eq. (26). The constants can be absorbed in the definition without any loss of generality. Using Eq. (25) we get

$$\Psi_1 = \sqrt{-g}[\rho_1 v_0^r H_{\theta 0} + \rho_0 v_1^r H_{\theta 0} + \rho_0 v_0^r H_{\theta 1}]. \tag{28}$$

The last term in Ψ_1 consists of a term with the perturbation of angular height function H_θ. We recall $H(r)$ as $H_\theta = H(r)/r$. For now, general height function $H(r)$ is used whereas later on we distinguish between conical flow and disc height proposed by Novikov and Thorne.

For adiabatic flow (8) can be rewritten as

$$h = 1 + \frac{\gamma}{\gamma - 1}\frac{p}{\rho} \tag{29}$$

where the perturbed quantity h_1 can be written as

$$h_1 = \frac{h_0 c_{s0}^2}{\rho_0}\rho_1. \tag{30}$$

For adiabatic flow the irrotationality condition is [24]

$$\partial_\mu(hv_\nu) - \partial_\nu(hv_\mu) = 0. \tag{31}$$

Now, by using Eq. (31), the normalization condition $v^\mu v_\mu = -1$, and the axial symmetry of the flow, we obtain quantities needed for further perturbation. From irrotaionality condition Eq. (31) with $\mu = t$ and $\nu = \phi$ and with axial symmetry we have

$$\partial_t(hv_\phi) = 0, \tag{32}$$

and for $\mu = r$ and $\nu = \phi$ and using axial symmetry, we have

$$\partial_r(hv_\phi) = 0. \tag{33}$$

So hv_ϕ is a constant of motion and Eq. (32) gives

$$\partial_t v_\phi = -\frac{v_\phi c_s^2}{\rho}\partial_t\rho. \tag{34}$$

Using $v_\phi = g_{\phi\phi}v^\phi + g_{\phi t}v^t$ in the previous equation gives

$$\partial_t v^\phi = -\frac{g_{\phi t}}{g_{\phi\phi}}\partial_t v^t - \frac{v_\phi c_s^2}{g_{\phi\phi}\rho}\partial_t\rho. \tag{35}$$

The normalization condition of four-velocity $v^\mu v_\mu = -1$ in this case can be written as

$$g_{tt}(v^t)^2 = 1 + g_{rr}(v^r)^2 + g_{\phi\phi}(v^\phi)^2 + 2g_{\phi t}v^\phi v^t. \tag{36}$$

The time derivative of this equation is

$$\partial_t v^t = \alpha_1\partial_t v^r + \alpha_2\partial_t v^\phi \tag{37}$$

where $\alpha_1 = -v_r/v_t$, $\alpha_2 = -v_\phi/v_t$, and $v_t = -g_{tt}v^t + g_{\phi t}v^\phi$. Replacing $\partial_t v^\phi$ in Eq. (37) and using Eq. (35) we get

$$\partial_t v^t = \left(\frac{-\alpha_2 v_\phi c_s^2/(\rho g_{\phi\phi})}{1 + \alpha_2 g_{\phi t}/g_{\phi\phi}}\right)\partial_t\rho + \left(\frac{\alpha_1}{1 + \alpha_2 g_{\phi t}/g_{\phi\phi}}\right)\partial_t v^r. \tag{38}$$

Using Eq. (25) in Eq. (38) and collecting the linear perturbation part we get

$$\partial_t v_1^t = \eta_1\partial_t\rho_1 + \eta_2\partial_t v_1^r \tag{39}$$

where

$$\eta_1 = -\frac{c_{s0}^2}{\Lambda v_0^t \rho_0}[\Lambda(v_0^t)^2 - 1 - g_{rr}(v_0^r)^2], \quad \eta_2 = \frac{g_{rr}v_0^r}{\Lambda v_0^t}$$
$$\text{and } \Lambda = g_{tt} + \frac{g_{\phi t}^2}{g_{\phi\phi}}. \tag{40}$$

Now we perturb height function and differentiate between the two models we consider. For conical flow, $H_{CF} = \Theta r$. Thus

$$(H_{\theta 1})_{CF} = 0. \tag{41}$$

For NT, $(H_{\theta 1})_{\rm NT}$ can be written as

$$\frac{(H_{\theta 1})_{\rm NT}}{(H_{\theta 0})_{\rm NT}} = \left(\frac{\gamma - 1}{2}\right)\frac{\rho_1}{\rho_0} = \beta_{\rm NT}\frac{\rho_1}{\rho_0} \tag{42}$$

where $\beta_{\rm NT} = \gamma - 1/2$. Here we see that the whole perturbation analysis can be generalized if we define $\beta_{CF} = 0$ for conical flow and continue the analysis with β in general. In the end we can again put these two different values and obtain different results for the two models.

The continuity equation takes the form

$$\partial_t(\sqrt{-g}\rho v^t H_\theta) + \partial_r(\sqrt{-g}\rho v^r H_\theta) = 0. \tag{43}$$

Using Eqs. (25) and (27) in the previous equation and using Eqs. (39) and (42) and replacing them in (43) yields

$$-\frac{\partial_r \Psi_1}{\Psi_0} = \frac{\eta_2}{v_0^r}\partial_t v_1^r + \frac{v_0^t}{v_0^r \rho_0}\left[1+\beta+\frac{\eta_1\rho_0}{v_0^t}\right]\partial_t\rho_1, \tag{44}$$

and

$$\frac{\partial_t \Psi_1}{\Psi_0} = \frac{1}{v_0^r}\partial_t v_1^r + \frac{1+\beta}{\rho_0}\partial_t\rho_1. \tag{45}$$

Using the two equations given by Eqs. (44) and (45) we can write $\partial_t v_1^r$ and $\partial_t\rho_1$ in terms of partial derivatives of Ψ_1 as

$$\begin{aligned}\partial_t v_1^r &= \frac{1}{\sqrt{-\tilde{g}}H_0\rho_0\tilde{\Lambda}}[(v_0^t(1+\beta)+\rho_0\eta_1)\partial_t\Psi_1 \\ &\quad + (1+\beta)v_0^r\partial_r\Psi_1], \\ \partial_t\rho_1 &= -\frac{1}{\sqrt{-\tilde{g}}H_0\rho_0\tilde{\Lambda}}[\rho_0\eta_2\partial_t\Psi_1 + \rho_0\partial_r\Psi_1]\end{aligned} \tag{46}$$

where $\tilde{\Lambda}$ is given by

$$\tilde{\Lambda} = (1+\beta)\left[\frac{g_{rr}(v_0^r)^2}{\Lambda v_0^t} - v_0^t\right] + \frac{c_{s0}^2}{\Lambda v_0^t}[\Lambda(v_0^t)^2 - 1 - g_{rr}(v_0^r)^2]. \tag{47}$$

Now we first linearly perturb Eq. (43) and then take its time derivative, which in turn gives

$$\begin{aligned}&\partial_t(h_0 g_{rr}\partial_t v_1^r) + \partial_t\left(\frac{h_0 g_{rr}c_{s0}^2 v_0^r}{\rho_0}\partial_t\rho_1\right) - \partial_r(h_0\partial_t v_{t1}) \\ &- \partial_r\left(\frac{h_0 v_{t0}c_{s0}^2}{\rho_0}\partial_t\rho_1\right) = 0.\end{aligned} \tag{48}$$

We can write

$$\partial_t v_{t1} = \tilde{\eta}_1\partial_t\rho_1 + \tilde{\eta}_2\partial_t v_1^r \tag{49}$$

with

$$\tilde{\eta}_1 = -\left(\Lambda\eta_1 + \frac{g_{\phi t}v_{\phi 0}c_{s0}^2}{g_{\phi\phi}\rho_0}\right), \qquad \tilde{\eta}_2 = -\Lambda\eta_2. \tag{50}$$

Using Eq. (49) in Eq. (48) and dividing it by $h_0 v_{t0}$ yields

$$\begin{aligned}&\partial_t\left(\frac{g_{rr}}{v_{t0}}\partial_t v_1^r\right) + \partial_t\left(\frac{g_{rr}c_s^2 v_0^r}{\rho_0 v_{t0}}\partial_t\rho_1\right) \\ &- \partial_r\left(\frac{\tilde{\eta}_2}{v_{t0}}\partial_t v_1^r\right) - \partial_r\left(\left(\frac{\tilde{\eta}_1}{v_{t0}} + \frac{c_s^2}{\rho_0}\right)\partial_t\rho_1\right) = 0\end{aligned} \tag{51}$$

where we use $h_0 v_{t0} =$ constant. Finally replacing $\partial_t v_1^r$ and $\partial_t\rho_1$ in Eq. (51) using Eq. (46) one obtains

$$\begin{aligned}&\partial_t\left[k(r)\left(-g^{tt} + (v_0^t)^2\left(1 - \frac{1+\beta}{c_s^2}\right)\right)\right] + \partial_t\left[k(r)\left(v_0^r v_0^t\left(1 - \frac{1+\beta}{c_s^2}\right)\right)\right] \\ &+ \partial_r\left[k(r)\left(v_0^r v_0^t\left(1 - \frac{1+\beta}{c_s^2}\right)\right)\right] + \partial_r\left[k(r)\left(g^{rr} + (v_0^r)^2\left(1 - \frac{1+\beta}{c_s^2}\right)\right)\right] = 0\end{aligned} \tag{52}$$

where $k(r)$ is a conformal factor whose exact form is not required for the present analysis.

Equation (52) can be written as

$$\partial_\mu(f^{\mu\nu}\partial_\nu\Psi_1) = 0 \tag{53}$$

where $f^{\mu\nu}$ is obtained from the symmetric matrix

$$f^{\mu\nu} = k(r)\begin{bmatrix} -g^{tt} + (v_0^t)^2(1 - \frac{1+\beta}{c_s^2}) & v_0^r v_0^t(1 - \frac{1+\beta}{c_s^2}) \\ v_0^r v_0^t(1 - \frac{1+\beta}{c_s^2}) & g^{rr} + (v_0^r)^2(1 - \frac{1+\beta}{c_s^2}) \end{bmatrix}. \tag{54}$$

Equation (53) describes the propagation of the perturbation Ψ_1 in $1+1$ dimensions effectively. Equation (53) has the same form of a massless scalar field in curved spacetime (with metric $g^{\mu\nu}$) given by

$$\partial_\mu(\sqrt{-g}g^{\mu\nu}\partial_\nu\varphi) = 0 \tag{55}$$

where g is the determinant of the metric $g_{\mu\nu}$ and φ is the scalar field. Comparing Eqs. (53) and (55), the components of acoustic spacetime metric $G_{\mu\nu}$ turns out to be

$$G_{\mu\nu}^{\mathrm{NT}} = k_1(r)\begin{bmatrix} -g^{rr} - (1 - \frac{1+\beta}{c_{s0}^2})(v_0^r)^2 & v_0^r v_0^t(1 - \frac{1+\beta}{c_{s0}^2}) \\ v_0^r v_0^t(1 - \frac{1+\beta}{c_{s0}^2}) & g^{tt} - (1 - \frac{1+\beta}{c_{s0}^2})(v_0^t)^2 \end{bmatrix} \tag{56}$$

where $k_1(r)$ is also a conformal factor arising due to the process of inverting $G^{\mu\nu}$ in order to yield $G_{\mu\nu}$. For our present purpose we do not need the exact expression for $k_1(r)$. The suffix "NT" is added because after the derivation of this acoustic metric, it is convenient to use just one β and the only flow with disc height as prescribed by Novikov and Thorne has nonzero β. Thus the above expression can now be used only to denote the acoustic metric for flow with height function as prescribed by Novikov and Thorne, whereas one can put $\beta = 0$ to get the acoustic metric for conical flow which is given by

$$G^{CF}_{\mu\nu} = k_1(r)\begin{bmatrix} -g^{rr} - (1-\frac{1}{c^2_{s0}})(v^r_0)^2 & v^r_0 v^t_0(1-\frac{1}{c^2_{s0}}) \\ v^r_0 v^t_0(1-\frac{1}{c^2_{s0}}) & g^{tt} - (1-\frac{1}{c^2_{s0}})(v^t_0)^2 \end{bmatrix}. \tag{57}$$

From the stationary solution of accretion flow, one expects the sonic point to be the acoustic horizon of the analog metric. But the nontrivial structure of the metric corresponding to flow with disc height as prescribed by Novikov and Thorne defined in Eq. (56) does not anymore assure that. Moreover, for both metrics, the particular coordinate assures that setting $G^{rr} = 0$ will determine the condition at acoustic black hole horizon. Thus we see that the condition at acoustic horizon for conical flow will be obtained by putting $\beta = 0$ in Eq. (54). This yields

$$g^{rr} + (v^r_0)^2\left(1 - \frac{1}{c^2_s}\right) = 0 \tag{58}$$

which in turn yields $u_0 = c_{s0}$ at the acoustic horizon. But the condition at acoustic horizon for flow with height prescription as proposed by Novikov and Thorne will be

$$g^{rr} + (v^r_0)^2\left(1 - \frac{1+\beta}{c^2_s}\right) = 0 \tag{59}$$

which in turn yields

$$u_0 = c_{s0}/\sqrt{1+\beta} \tag{60}$$

at the acoustic horizon. For later purposes it will be convenient to define an effective sound speed

$$c_{\text{eff}} = c_{s0}/\sqrt{1+\beta} \tag{61}$$

for flow with height as prescribed by Novikov and Thorne and $c_{\text{eff}} = c_{s0}$ for conical flow.

V. CARTER-PENROSE DIAGRAM OF THE ACOUSTIC METRICS FOR POLYTROPIC ACCRETION

The redefinition of sound speed as performed in the previous section was motivated using the local conditions at black hole horizons. One may formally analyze the causal structure of the acoustic spacetime of the models to find the location of the horizon. In this process the global features of light cones at any point in the acoustic sapcetime will then justify the redefinition of sound speed anywhere in the flow and not only at the acoustic black hole horizons. Thus in this section, we will study the causal structure by numerically plotting the Carter-Penrose diagram [67] of the acoustic metric. The method of the Carter-Penrose diagram is used in general relativity to understand the global features of complicated black hole spacetimes like Kerr spacetime and it is also used in cosmology [68]. Here we will use the Carter-Penrose diagram as it is used in the context of black hole spacetimes to determine black hole and white hole regions. The Carter-Penrose diagram of the analog metric has been done in [69], where constant sound speed was used and the flow profiles were assumed instead of being derived from some fluid or any other underlying set of governing equations. In our analysis, the sound speed is a local function of radial distance and the flow profile was solved from the governing equations. The nontrivial discontinuous transition of the fluid profiles from the supersonic region to the subsonic region at the shock location is also the result of the physical process determined by Rankine-Hugoniot conditions. These kinds of complexities were not considered previously in the causal structure analysis of acoustic spacetimes.

In this section we first simplify the metric elements in terms of stationary fluid variables and then apply proper coordinate transformations to remove the coordinate singularities of the metrics. Then those coordinates are further transformed to compactify the entire analog spacetime. Next we plot the Carter-Penrose diagram for both the models, define the boundaries from the point of view of differential geometry, and then use a causal relation to find out the features of different regions of the analog spacetime corresponding to different parts of the fluid flow. From this analysis the redefinition of sound speed will be justified globally.

A. Acoustic metric and other preliminaries

From the obtained acoustic metric the line element is given by

$$ds^2 = G_{tt}dt^2 + 2G_{tr}dtdr + G_{rr}dr^2, \tag{62}$$

where the metric elements $G_{\mu\nu}$ are given by (57) and (56). The overall factor $k_1(r)$ is not explicitly taken into account as we want to finally focus on a conformally transformed

metric where this factor can be absorbed with the conformal factor.

Using Eq. (6) and the contravariant form of Eq. (5), the metric elements of acoustic matrices turn out to be

$$G_{tt} = \frac{u_0^2 - c_{\text{eff}}^2}{c_{\text{eff}}^2(1-u_0^2)g_{rr}},$$
$$G_{tr} = G_{rt} = \frac{u_0(1-c_{\text{eff}}^2)F_1(r,\lambda)}{c_{\text{eff}}^2(1-u_0^2)},$$
$$G_{rr} = \frac{g_{rr}F_1^2(r,\lambda)(1-c_{\text{eff}}^2)}{c_{\text{eff}}^2(1-u_0^2)} - F_2(r), \tag{63}$$

where

$$F_1(r,\lambda) = \frac{g_{\phi\phi} + \lambda g_{\phi t}}{\sqrt{(g_{\phi\phi} + 2\lambda g_{\phi t} - \lambda^2 g_{tt})(g_{\phi\phi}g_{tt} + g_{\phi t}^2)g_{rr}}},$$
$$F_2(r) = \frac{g_{\phi\phi}}{g_{\phi\phi}g_{tt} + g_{\phi t}^2}. \tag{64}$$

Thus we see that at a critical point where $u_0^2 = c_{\text{eff}}^2$, the metric element G_{tt} becomes zero. So we have to transform the coordinate so that the coordinate singularity is removed. In the next section, we go through a systematic procedure such that the singularity is removed from new metric elements. In this new set of coordinates the spacetime represented by an acoustic metric extends up to infinity. Thus we will conformally transform these coordinates such that the infinite spacetime is mapped into a finite region of some coordinate space. As mentioned in the Introduction, this conformal transformation and the corresponding Carter-Penrose diagram will help one to study the causal structure of the acoustic spacetime.

B. Kruskal-like coordinate transformation to remove singularity at critical points

The general transformations that lead to the construction of Carter-Penrose diagrams in the context of black hole metrics has been studied in detail in [67,68]. The corresponding transformations in the context of an analog metric has been derived in [69]. Although we follow the general outline, the acoustic metric derived by us has the special feature of sound speed being a function of radial distance r. Thus the coordinate transformations are more involved and the procedure is described in this section in details.

First we choose null coordinates to write down the line element (62). We note that for null or lightlike curves $ds^2 = 0$, which yields

$$(dt - A_+(r)dr)(dt - A_-(r)dr) = 0 \tag{65}$$

where

$$A_\pm = \frac{-G_{tr} \pm \sqrt{G_{tr}^2 - G_{rr}G_{tt}}}{G_{tt}}. \tag{66}$$

So instead of coordinates (t, r), we choose new coordinates to be null coordinates (χ, ω) such that

$$d\omega = dt - A_+(r)dr, \tag{67}$$

$$d\chi = dt - A_-(r)dr. \tag{68}$$

Using the coordinate transformation introduced in (67), the line element (62) can be written as

$$ds^2 = G_{tt}d\chi d\omega. \tag{69}$$

After introducing the null coordinates, the next step usually should be the affine parametrization, which removes the removable singularity. But one can remove the singularities of G_{tt} at the critical points by observing how the divergence behaves at the vicinity of the horizon. To study this behavior we expand $A_-(r)$ and $A_+(r)$ up to first order of $(r - r_c)$. Thus by expanding u_0 near r_c as

$$u_0(r) = -c_{\text{eff}}(r_c) + \left|\frac{du}{dr}\right|_{r_c}(r - r_c) + O((r - r_c)^2) \tag{70}$$

where the negative sign of the effective sound speed implies the flow is toward the accretor. We also note that from(70), near r_c we can write

$$u_0^2 - c_{\text{eff}}^2 \approx -2\left(c_{\text{eff}}\frac{du}{dr}\right)_{r_c}(r - r_c) \tag{71}$$

considering up to the first order term.

Now we expand $A_-(r)$ and $A_+(r)$ up to linear order of $(r - r_c)$. For that we first note that $G_{tt} \propto (u_0 - c_{\text{eff}})^2$ is very small near r_c which implies $|G_{tt}G_{rr}/G_{tr}^2| \ll 1$. Thus we obtain

$$A_+(r) = \frac{-G_{tr} + G_{tr}(1 - \frac{G_{tt}G_{rr}}{G_{tr}^2})^{1/2}}{G_{tt}} \tag{72}$$

$$\approx -\frac{G_{rr}}{2G_{tr}} \tag{73}$$

and

$$A_-(r) = \frac{-G_{tr} - G_{tr}(1 - \frac{G_{tt}G_{rr}}{G_{tr}^2})^{1/2}}{G_{tt}} \tag{74}$$

$$\approx -\frac{2G_{tr}}{G_{tt}} \tag{75}$$

$$= \frac{2F_1(r,\lambda) g_{rr} u_0 (c_{\rm eff}^2 - 1)}{u_0^2 - c_{\rm eff}^2} \tag{76}$$

$$\approx \frac{F_1(r_c,\lambda) g_{rr} (u_{0c}^2 - 1)}{u'_{0c} - (c'_{\rm eff})_c} \frac{1}{r - r_c} \tag{77}$$

$$= \frac{1}{\kappa} \frac{1}{r - r_c} \tag{78}$$

where

$$\kappa = \frac{u'_{0c} - (c'_{\rm eff})_c}{F_1(r_c,\lambda) g_{rr} (u_{0c}^2 - 1)}. \tag{79}$$

So, we see that although

$$\chi \approx t - \frac{1}{\kappa} \ln |r - r_c| \tag{80}$$

shows a logarithmic divergence at $r \to r_c$, the form of G_{rr} and G_{tr} ensures that

$$\omega = t + \int \frac{G_{rr}}{2G_{tr}} dr \tag{81}$$

does not diverge at the critical points as the function inside the integral is regular there.

Thus we see that near the critical points

$$e^{-\kappa\chi} \propto e^{-\kappa t} |r - r_c| \propto e^{-\kappa t} (u_0^2 - c_{\rm eff}^2). \tag{82}$$

Now one can compare the acoustic null coordinates in this case with that of the Schwarzchild metric and guess a coordinate transformation such that the singularity of the metric element at the critical point is removed. The transformation equations can be given by

$$\begin{aligned} U(\chi) &= -e^{-\kappa\chi}, \\ W(\omega) &= e^{\kappa\omega}. \end{aligned} \tag{83}$$

Using this new set of coordinates (U, W), the line element can now be written as

$$ds^2 = G_{tt} \frac{e^{\kappa(\chi-\omega)} (u_0^2 - c_{\rm eff}^2)}{\kappa^2 c_{\rm eff}^2 (1 - u_0^2)(1 - 2/r + a/r^2)^{-1}} dU dW. \tag{84}$$

Thus at the numerator of the new metric element, the two factors multiplied together will cancel the divergence at critical points. Thus these new coordinates (U, W) are similar to the Kruskal coordinates for the case of the Schwarzchild metric which removes the coordinate singularity.

Now we have to compactify the infinite space into a finite patch of some coordinates. For that, the coordinates will be (T, R) such that

$$T = \tan^{-1}(W) + \tan^{-1}(U), \tag{85}$$

$$R = \tan^{-1}(W) - \tan^{-1}(U). \tag{86}$$

Just like one would plot $r =$ constant lines in the Kruskal coordinate plane to get the Kruskal diagram, $r =$ constant, lines can be drawn in these (T, R) coordinates, and the resulting diagram would be able to represent causal structure of the original spacetime in a compactified region. The resulting diagram in (T, R) coordinates is technically known as the Carter-Penrose diagram.

Now we write down how the original metric defined in Eq. (62) is transformed when we express it in terms of T and R and comment on the structure of the metric. The metric ds^2 in terms of T and R is

$$ds^2 = \Omega^2 (-dT^2 + dR^2) \tag{87}$$

where

$$\Omega^2 = -G_{tt} \sec^2\left(\frac{T+R}{2}\right) \sec^2\left(\frac{T-R}{2}\right) \frac{e^{\kappa(\chi-\omega)} (u_0^2 - c_{\rm eff}^2)}{4\kappa^2 c_{\rm eff}^2 (1 - u_0^2)(1 - 2/r + a/r^2)^{-1}}. \tag{88}$$

We thus see from Eq. (87) that we have finally obtained the transformations that connect the original metric conformally with the two-dimensional Minkwoski metric, where two metrics G and g on the same manifold $\mathcal{M}$ are said to be conformally connected if there is a positive definite conformal factor $\Omega^2(x)$ such that

$$G_{\mu\nu} dx^\mu \otimes dx^\nu = \Omega^2(x) g_{\mu\nu} dx^\mu \otimes dx^\nu. \tag{89}$$

This conformal connection of the metric of analog spacetime with two-dimensional Minkowski spacetime will be the key point to establishing causal significance of interesting features in analog spacetimes presented earlier.

C. Carter-Penrose diagram

In order to draw the Carter-Penrose diagram, the multitransonic flow lines chosen previously are used as the background flow. Then the stationary metric elements are

generated as a function of the r coordinate, i.e., the metric elements $G_{\mu\nu}$ are defined numerically on the analog spacetime in (t, r) coordinates. Then by the prescribed transformations as formulated in the previous subsection, $r =$ constant lines are plotted in the (T, R) plane, generating the Carter-Penrose diagram which transforms the infinite (t, r) plane into a finite region of the (T, R) plane. The diagrams are obtained for adiabatic flow with both conical disc height and height function as prescribed by Novikov and Thorne. The corresponding plots are presented in Fig. 2 for both the geometries.

In order to understand the significance of the compactification which is presented in the Carter-Penrose diagram and to classify the regions corresponding to the black hole and the white hole, one must understand the causal significance of the boundaries of the compactified diagrams. Once we define different parts of the boundaries, which already requires the understanding of the causal relationship between two points in a spacetime, we will use the relationships on entire boundaries and see how the definitions of black hole and white hole regions arise naturally along with the corresponding horizons.

In order to understand why the compactification makes it easy to analyze causal structures from the compactified Carter-Penrose diagrams, we must first state a lemma from the theory of differential manifolds that relates the behavior of null geodesics in analog spacetime with the behavior of null geodesics in Minkowski spacetime. The lemma states the following [68]:

Lemma.—If two matrices G and g on the same manifold $\mathcal{M}$ are conformally related [as defined in Eq. (89)], then the null geodesics with respect to metric G are null geodesics also with respect to the metric g and vice versa.

It was established in Eq. (87) that the analog metric derived in Eqs. (57) and (56) for the multitransonic flow chosen previously is conformally flat, i.e., the resulting analog metric is conformally connected with flat or Minkowski spacetime. Thus the sound cones in these compactified diagrams will have the same orientation as light cones in Minkowski spacetime. So the sound cones in the compactified diagrams at an angle of $\pi/4$ and $3\pi/4$ to the horizontal lines if the scale of both T and R are the same. This orientation of sound cones is global.

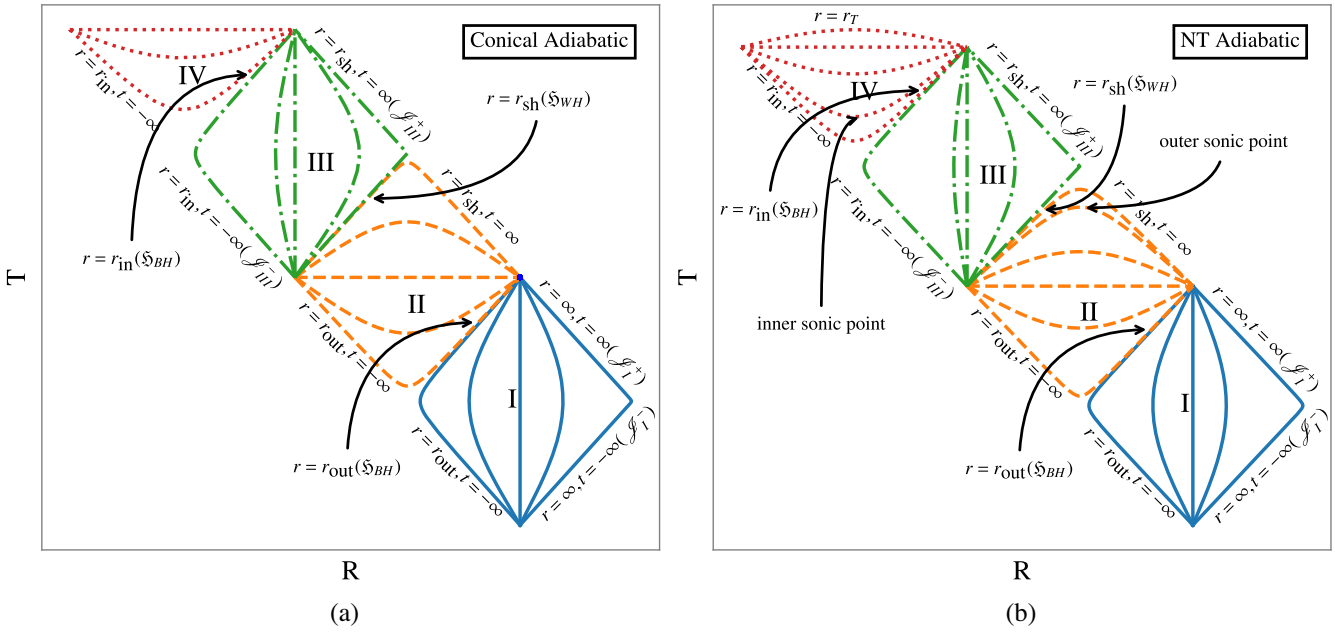

FIG. 2. (a) Carter-Penrose diagram for adiabatic flow with conical disc height. (b) Carter-Penrose diagram for adiabatic flow with height expression formulated by Novikov and Thorne. In both Carter-Penrose diagrams for adiabatic flow, region I marked with blue solid lines corresponds to the flow outside the outer critical point r_{out} up to infinity, where flow is subsonic. Region II marked with yellow dashed lines corresponds to the flow inside r_{out} and outside r_{shock}, where flow is supersonic. Region III marked with green dash-dotted lines corresponds to the flow inside the shock r_{shock} and outside the inner critical point r_{in}, where flow is again subsonic. Region IV marked with red dotted lines corresponds to the flow inside the inner critical point r_{in} up to the minimum radius where flow can be extended outside the real Kerr black hole horizon and the flow is supersonic again. All of the lines correspond to $r =$ constant lines in their corresponding regions expect for the lines at boundaries where the $r =$ constant lines coincide with $t =$ constant lines where the time values are as specified in the figures. For flow with height functions prescribed by Novikov and Thorne, the $r =$ constant lines corresponding to usual sonic points are shown.

The simple orientation of a light cone in a Carter-Penrose diagram makes it easy to understand how timelike, spacelike, and null vectors will be oriented, as they are just similar to the definition of vectors in two-dimensional Minkowski spacetime. The vectors at any point in these diagrams will be timelike if they are inside the sound cone, null if they are on the boundaries of the sound cone, and spacelike if they are outside the sound cone.

With these definitions of the causal nature of vectors in mind we can now define causal curves in a manifold $\mathcal{M}$. A curve $\lambda(s)$ in any manifold $\mathcal{M}$ is a causal curve if for every point $p \in \lambda$ the tangent vector t^μ at that point is timelike or null. This definition of causal curve enables us to define the causal future/past of a point p. The causal future/past of a point p, denoted by $J^\pm(p)$, is a subset of $\mathcal{M}$ defined by the following condition:

$$J^\pm(p) = \{q \in \mathcal{M} | \exists \text{ future-(past-) directed causal curve } \lambda(s) \text{ such that } \lambda(0) = p; \lambda(1) = q\}. \tag{90}$$

The causal future/past of a region will be the union of causal future/past of all the points belonging to the region.

In Sec. V B, we defined the set of transformations that transform the (t, r) coordinates into (T, R) coordinates. Thus we get an image of the (t, r) plane in the (T, R) plane. Denoting this transformation or mapping ψ, we see that the mapping is injective but not surjective, i.e., the image of the entire (t, r) plane is a subset of the (T, R) plane, which represents the two-dimensional Minkwoski plane as can be seen from the signatures in the metric. Now the boundaries at infinity have been brought to finite distances and thus the boundary of this mapping in this finite domain can be analyzed causally. We define the boundary of the mapping ψ of the entire analog spacetime $\mathcal{M}$ as

$$\partial\psi(\mathcal{M}) = i^0 \cup \mathcal{J}^+ \cup \mathcal{J}^- \tag{91}$$

where

(1) i_0, known as *spatial infinity*, is the endpoint of the ψ image of all spacelike curves in $(\mathcal{M}, g)$;
(2) $\mathcal{J}^+$, known as *future causal infinity*, is the endpoint of the ψ image of all future-directed causal curves in $(\mathcal{M}, g)$;
(3) $\mathcal{J}^-$, known as *past causal infinity*, is the endpoint of the ψ image of all past directed causal curves in $(\mathcal{M}, g)$.

In order to specify the boundaries of the Carter-Penrose diagram as shown in Fig. 2, it must be noted that the whole diagram consists of four regions, denoted by I, II, III, and IV. Regions I and III are subsonic, keeping in mind that we do not anymore consider the usual sound speed as defined in Eq. (7) to separate between the subsonic region and supersonic region and consider the effective sound speed, by allowing the phonons to propagate freely in any direction. Thus both of these regions have future and past causal infinities as their boundaries. These causal infinities are numerically generated by setting the time to be very large positive or negative numbers. The future null infinities for region I and region III are denoted by $\mathcal{J}^+_{\mathrm{I}}$ and $\mathcal{J}^+_{\mathrm{III}}$ respectively. Similarly, the past null infinities for region I and region III are denoted by $\mathcal{J}^-_{\mathrm{I}}$ and $\mathcal{J}^-_{\mathrm{III}}$ respectively.

Now the concepts of causal future and past are applied on the boundaries of the Carter-Penrose diagrams to find black hole and white hole regions formally. But before we delve into that an observation from the Carter-Penrose diagrams should be noted. When we define a region as a black hole or white hole in analog spacetime, it is done with respect to either region I or region III. As previously mentioned, both regions I and III are subsonic, making them similar to regions of a universe outside any kind of horizons. But as we see from the Carter-Penrose diagrams, the two regions are connected by region II. As region II corresponds to supersonic flow, we can guess that this region will be a black hole or a white hole. As we will see next, this region can be denoted as a black hole or white hole region both, but it depends on the region with respect to which we define its properties.

Now we focus on the features of region II and region IV. We find that the intersection of region II with the causal past of future null infinity of region I is null, i.e., $\mathrm{II} \cap J^-(\mathcal{J}^+_{\mathrm{I}}) = \varnothing$. Similarly we have $\mathrm{IV} \cap J^-(\mathcal{J}^+_{\mathrm{III}}) = \varnothing$. This property establishes a formal mathematical definition of a region which can be defined as cut off from communication from the rest of the universe. As is intuitively known, the black hole region is characterized by this property of being cut off from the rest of the universe. Region II is cut off from region I and region IV is cut off from region III. Thus region II is a black hole region as perceived from an observer in region I, and region IV is a black hole region as perceived from region III. But as previously mentioned, in the context of analog gravity, this property of region II does not make it a black hole universally and it can only be termed black hole from the point of view of an observer in region I. But the black hole horizons $\mathfrak{H}_{\mathrm{BH}}$, the boundary of the black hole region separating it from the causal past of future null infinity, is a hypersurface whose definition does not require the specification of where the observer is located explicitly. Thus this particular causal boundary which is denoted as a black hole horizon separates an black hole from its corresponding universe, or in terms of acoustic geometry with which we are concerned at this moment, the acoustic horizon is the barrier between a subsonic and supersonic region where we

take the definition of effective sound speed as defined in Eq. (61) into consideration while we define a region to be subsonic or supersonic. Mathematically, the definition of a black hole horizon translates to

$$\mathfrak{H}_{\rm BH} = \partial BH \cap \partial J^{-}(\mathcal{J}^{+}), \tag{92}$$

where ∂ denotes the boundary of the respective region.

From the definition of the black hole horizon, inspection of Fig. 2 implies that for both models, there are two black hole horizons for the individual model we chose. One of them is the boundary between region I and II, i.e., the outer critical point $r_{\rm out}$ and the other one is the boundary between region III and region IV, i.e., the inner critical point $r_{\rm in}$. This identification is true for accretion flow with conical height function as well as flow with height function as prescribed by Novikov and Thorne. In the case of Carter-Penrose diagram for conical flow, the boundary of region I and region II denotes the critical or sonic points which are the same in this case. But for flow with height prescription as described by Novikov and Thorne, if the modified sound speed is not used, then we see that the line "$r =$ outer sonic point" lies inside region II as has been pointed out. Thus, in this case, the sonic point does not act as the deciding boundary of propagation for linear perturbation. Thus the redefinition of effective sound speed is justified and one can use this definition not only at the horizon as motivated previously, but also this redefinition can be done in the entire acoustic spacetime or throughout the manifold where the flow is defined.

Now we focus on the causal significance of region II as observed from the point of view of an observer in region III. We find that the intersection of region II with the causal future of past null infinity of region III is null, i.e., $\mathrm{II} \cap J^{+}(\mathcal{J}^{+}_{\rm III}) = \varnothing$. This property establishes a formal mathematical definition of a region to which the universe can never communicate. But unlike the black hole, communication can be sent from the aforementioned region to its corresponding universe. Thus region II intuitively resembles the definition of a white hole in which no signal can be sent from the universe, i.e., region III but signals can reach to region III from region II. Here also the definition of the white hole horizon $\mathfrak{H}_{WH}$ as the boundary of the white hole region separating it from the causal future of past null infinity does not require the specification of the position of an observer explicitly. Mathematically, the definition of the white hole horizon translates to

$$\mathfrak{H}_{WH} = \partial WH \cap \partial J^{+}(\mathcal{J}^{-}). \tag{93}$$

From our discussion on the definition of a black hole, we see there is no event in the black hole region which causally affects any events in the corresponding universe. In the case of a white hole, there is no event in the corresponding universe that will ever causally affect any event inside the white hole. It is evident that if the definition of modified sound speed is used then the critical points will act as the acoustic black hole horizon. The motivation for invoking the Carter-Penrose diagram techniques to analog spacetime was to establish the crucial role of critical points, but the role of shock as a white whole horizon is not a feature that could be readily anticipated. In [46] Abraham *et al.* invoked the techniques of analog gravity to establish that shocks act as white holes by invoking a certain quantity which goes to zero at the white hole horizon. Constant height of accretion disc in Kerr spacetime was used in this work. Here we conclude the same thing but the connection between Rankine-Hugoniot conditions and causal feature of the location of the shock as established from our analysis with Carter-Penrose diagram can further be studied.

VI. PHASE PORTRAIT AND CARTER-PENROSE DIAGRAM FOR ISOTHERMAL FLOW

The problem of nonisomorphism of critical points and sonic points for adiabatic flow with height function as prescribed by Novikov and Thorne was solved by invoking the definition of effective sound speed and establishing its global significance by causal structure analysis of a Carter-Penrose diagram. But we found that not only does this solve the aforementioned nonisomorphism problem, but it also establishes shock as a white hole horizon. Thus the causal significance that can be extracted by analyzing a Carter-Penrose diagram is independent of the occurrence of any problem and can be pursued for its own merit to analyze analog spacetime. Thus the previously used framework on the adiabatic flow can be used to analyze the analog metric emerging from the isothermal flow also. In this section we present the phase portraits for isothermal flow and find that the problem of nonisomorphism of critical points and sonic points are not present for isothermal flow. After we present the stationary solutions and choose shocked multitransonic flow as before, the framework for Carter-Penrose diagram is used and the corresponding diagrams are presented.

Now for isothermal flow, the governing fluid equations will have the same form as used in adiabatic flow. The characteristic of isothermal flow will be manifested in the results by the equation of state, given by

$$p = c_s^2 \rho = \frac{\mathcal{R}}{\mu}\rho T = \frac{k_B \rho T}{\mu m_H} \tag{94}$$

where T is the bulk ion temperature, $\mathcal{R}$ is the universal gas constant, k_B is the Boltzmann constant, m_H is the mass of the hydrogen atom, and μ is the mean molecular mass of a fully ionized hydrogen atom. Now integrals of motions must be constructed as was done for adiabatic flows.

A. Phase portrait

The first conserved quantity obtained by integrating Euler equation (11) turns out to be

$$\xi = v_t \rho^{c_s^2} = \rho^{c_s^2} \sqrt{\frac{\Delta}{B(1-u^2)}}. \tag{95}$$

The second constant of integration obtained by integrating the continuity equation has the same form as described for polytropic accretion, given by Eq. (18).

Now using these two constant of integration, we can obtain the derivative of advective velocity u_0 for isothermal flow as was done for polytropic flow. The expression for a derivative of advective velocity corresponding to conical height function given by Eq. (12) turns out to be (see [62])

$$\left.\frac{du_0}{dr}\right|_{CF}^{\text{iso}} = \frac{u_0(1-u_0^2)[c_{s0}^2 \frac{2r^2-3r+a^2}{\Delta r} + \frac{1}{2}(\frac{B'}{B} - \frac{\Delta'}{\Delta})]}{u_0^2 - c_{s0^2}} = \left.\frac{N_{CF}}{D_{CF}}\right|^{\text{iso}}. \tag{96}$$

The expression of derivative for height function (see [24]) as prescribed by Novikov and Thorne given by Eq. (13) is

$$\left.\frac{du_0}{dr}\right|_{\text{NT}}^{\text{iso}} = \frac{u_0(1-u_0^2)[c_{s0}^2(\frac{\Delta'}{2\Delta} + \frac{f'}{f}) + \frac{1}{2}(\frac{B'}{B} - \frac{\Delta'}{\Delta})]}{u_0^2 - c_{s0}^2} = \left.\frac{N_{\text{NT}}}{D_{\text{NT}}}\right|^{\text{iso}}. \tag{97}$$

Now we see that for isothermal flow, one does not anymore have to worry about the issue of sonic points and critical points not being the same as is evident from inspection of the denominator of both the derivatives stated above. Thus we will expect that a Carter-Penrose diagram will also establish this trivial feature and there is no need to differentiate between the sound speed and the speed of propagation of the first order perturbation in the accreting matter.

We present the phase portraits for isothermal flow for both the conical disc height and flow with height prescription as described by Novikov and Thorne in Fig. 3.

From the family of phase portraits, only critical flows have been demonstrated in Fig. 3. We will again choose the accretion flow from well outside the outer critical point, passing through the outer critical point to the shock, making a discontinuous jump from the outer accretion branch to the inner accretion branch and then again becoming transonic at the inner critical point and flowing inside it. The purpose of this is again to obtain transonic flow.

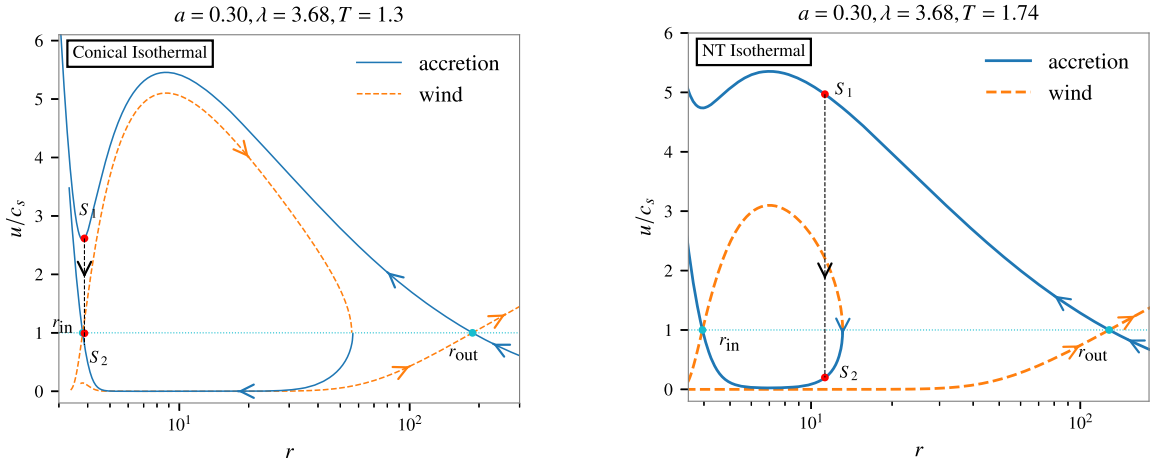

FIG. 3. (a) Phase portrait for isothermal flow with conical disc height. (b) Phase portrait for isothermal flow with height expression formulated by Novikov and Thorne. Both phase portraits have been drawn for isothermal accretion with the set of parameter values $\lambda = 3.68$ and $a = 3.0$. The temperatures are written in the unit of 10^{10} K. For both pictures the blue solid lines correspond to the accretion branch whereas the orange dashed lines correspond to the wind branch. The innermost critical point is denoted as r_{in} and outermost critical point is denoted as r_{out}. S_1 corresponds to the point in the phase portrait in the accretion branch through the outer critical point where the shock may occur and S_2 corresponds to the point where the shock occurs in the accretion branch through the inner critical point. The same radial distance of S_1 and S_2 corresponds to the fact that the shock is infinitesimally thin. The dotted black line joining S_1 and S_2 corresponds to the discontinuous jump in the shock location. For both conical flow and flow with height as formulated by Novikov and Thorne, the sonic points and critical points coincide in the case of isothermal flow. The two points r_{in} and S_2 do not coincide in (a), although it may seem so from the figure as the radial distance between the two is very small.

B. Linear perturbation scheme for isothermal flow

The perturbation scheme will be the same as the one used in the polytropic flow and the time-dependent accretion variables are again small time-dependent linear perturbations added to the time-independent stationary values as described in Eq. (25).

1. Perturbation of Euler equation or the irrotationality condition

For isothermal flow, the irrotationality condition turns out to be [50]

$$\partial_\mu(\rho^{c_s^2} v_\nu) - \partial_\nu(\rho^{c_s^2} v_\mu) = 0 \tag{98}$$

which can be obtained from the equation of state for isothermal flow along with the two fluid equations. From the irrotationality condition [Eq. (98)] with $\mu = t$ and $\nu = \phi$ and with axial symmetry we have

$$\partial_t(h v_\phi) = 0, \tag{99}$$

and, for $\mu = r$ and $\nu = \phi$ and the axial symmetry, we have

$$\partial_r(\rho^{c_s^2} v_\phi) = 0. \tag{100}$$

So $\rho^{c_s^2} v_\phi$ is a constant of motion and Eq. (99) gives

$$\partial_t v_\phi = -\frac{v_\phi c_s^2}{\rho}\partial_t \rho, \tag{101}$$

which has exactly the same form as Eq. (34), although in the case of isothermal flow, c_s is a constant whereas it was a function of radial distance in the case of adiabatic flow. As Eqs. (35)–(40) are derived from Eq. (34), and they are not dependent on the geometry on the disc, rather on the background Kerr metric elements, these equations will remain the same for isothermal flow.

2. Perturbation of continuity equation

In the case of isothermal flow for accretion disc in hydrostatic equilibrium along the vertical direction, i.e., disc with height function as prescribed by Novikov and Thorne, we have

$$H(r) = \left(\frac{p}{\rho}\right)^{\frac{1}{2}} f(r) = c_s^2 f(r) = F(r) \tag{102}$$

where $F(r)$ is purely a function of radial distance as sound speed c_s is a constant in the case of isothermal flow. In the case of conical flow, the height function is anyway a completely radial function where height does not depend on the flow variable. Thus we do not need separate treatment for perturbation in the case for isothermal flow, as was necessary for adiabatic flows. Henceforth for the isothermal case

$$H_{\theta 1}(r) = \frac{H_1(r)}{r} = 0. \tag{103}$$

Thus the perturbed mass accretion rate here will have the form

$$\Psi_1 = \sqrt{-g}[\rho_1 v_0^r H_{\theta 0} + \rho_0 v_1^r H_{\theta 0}] \tag{104}$$

instead of Eq. (28), which represented this perturbed quantity in the case of adiabatic flow in hydrostatic equilibrium.

Using the definition of Ψ and Ψ_1 from Eqs. (26) and (104) in Eq. (43),one yields

$$-\frac{\partial_r \Psi_1}{\Psi_0} = \frac{\eta_2}{v_0^r}\partial_t v_1^r + \frac{v_0^t}{v_0^r \rho_0}\left[1 + \frac{\eta_1 \rho_0}{v_0^t}\right]\partial_t \rho_1, \tag{105}$$

and taking the time derivative of Eq. (104), one yields

$$\frac{\partial_t \Psi_1}{\Psi_0} = \frac{1}{v_0^r}\partial_t v_1^r + \frac{\partial_t \rho_1}{\rho_0} \tag{106}$$

instead of Eqs. (44) and (45).

We see that Eqs. (105) and (106) are basically Eqs. (44) and (45) with $\beta = 0$. The reason for this is that there is no contribution of the first order perturbation of height function in the perturbation of mass accretion rate in Eq. (104) as was the case in Eq. (28).

Thus Eqs. (46) and (47) will be applicable for the isothermal flow with $\beta = 0$.

Now putting $\mu = t$ and $\nu = r$ in the irrotatonality condition for isothermal flow, i.e., Eq. (98), it is linearly perturbed and the time derivative is taken. This yields

$$\partial_t(\rho_0^{c_s^2} g_{rr}\partial_t v_1^r) + \partial_t\left(\frac{\rho_0^{c_s^2} g_{rr} c_{s0}^2 v_0^r}{\rho_0}\partial_t \rho_1\right) - \partial_r(\rho_0^{c_s^2}\partial_t v_{t1}) - \partial_r\left(\frac{\rho_0^{c_s^2} v_{t0} c_{s0}^2}{\rho_0}\partial_t \rho_1\right) = 0. \tag{107}$$

which exactly resembles Eq. (48), if h_0 in the aforementioned equation for adiabatic flow is replaced by $\rho_0^{c_s^2}$ for the isothermal case here. Now using Eq. (49) in Eq. (107), and dividing the equation by $\rho_0^{c_s^2}$ one yields Eq. (51) again. Thus using $\partial_t v_1^r$ and $\partial_t \rho_1$ in Eq. (51) using Eq. (46) with $\beta = 0$ one obtains

$$\partial_t\left[k(r)\left(-g^{tt}+(v_0^t)^2\left(1-\frac{1}{c_s^2}\right)\right)\partial_t\Psi_1\right]+\partial_t\left[k(r)\left(v_0^r v_0^t\left(1-\frac{1}{c_s^2}\right)\right)\partial_r\Psi_1\right]$$
$$+\partial_r\left[k(r)\left(v_0^r v_0^t\left(1-\frac{1}{c_s^2}\right)\right)\partial_t\Psi_1\right]+\partial_r\left[k(r)\left(g^{rr}+(v_0^r)^2\left(1-\frac{1}{c_s^2}\right)\right)\partial_r\Psi_1\right]=0 \tag{108}$$

where $k(r)$ is a conformal factor whose exact form is not required for the present analysis, as mentioned in the case of adiabatic flow. Equation (52) can be written in the form of wave equation (53), where in the case of isothermal flow $f^{\mu\nu}$ is given by

$$f^{\mu\nu}=k(r)\begin{bmatrix}-g^{tt}+(v_0^t)^2(1-\frac{1}{c_s^2}) & v_0^r v_0^t(1-\frac{1}{c_s^2})\\ v_0^r v_0^t(1-\frac{1}{c_s^2}) & g^{rr}+(v_0^r)^2(1-\frac{1}{c_s^2})\end{bmatrix}. \tag{109}$$

The acoustic spacetime $G_{\mu\nu}$ metric in the case of isothermal flow thus turns out to be

$$G_{\mu\nu}=k_1(r)\begin{bmatrix}-g^{rr}-(1-\frac{1}{c_{s0}^2})(v_0^r)^2 & v_0^r v_0^t(1-\frac{1}{c_{s0}^2})\\ v_0^r v_0^t(1-\frac{1}{c_{s0}^2}) & g^{tt}-(1-\frac{1}{c_{s0}^2})(v_0^t)^2\end{bmatrix} \tag{110}$$

where $k_1(r)$ is the previously mentioned conformal factor arising due to the process of inverting $G^{\mu\nu}$ in order to yield $G_{\mu\nu}$. Again we do not need the exact expression for $k_1(r)$.

C. Carter-Penrose diagram of acoustic metric for isothermal flow

The construction of Carter-Penrose diagrams are exactly the same as described for the case of adiabatic flow. All the coordinate transformations are the same once one obtains the acoustic metric for a flow. The effective sound speed is the same as the usual stationary thermodynamic definition of sound speed in the case of isothermal accretion. The qualitative feature for the Carter-Penrose diagram is the same as what was illustrated in the case of adiabatic flow. Here also multitransonicity gives rise to a pair of black holes connected by shock as illustrated in Fig. 4. The similarity of the qualitative nature of the Carter-Penrose diagrams invoke similar causal analysis as was done for adiabatic flow. The difference between the Carter-Penrose

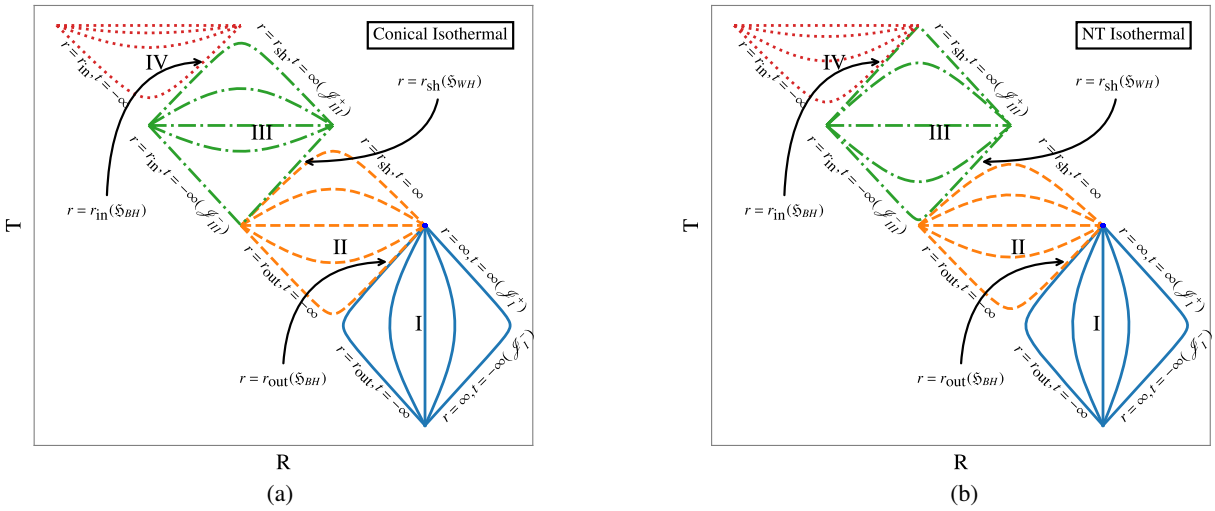

FIG. 4. (a) Carter-Penrose Diagram for isothermal flow with conical disc height. (b) Carter-Penrose diagram for isothermal flow with height expression formulated by Novikov and Thorne. In both the Carter-Penrose diagrams for isothermal flow, region I marked with blue solid lines corresponds to the flow outside the outer critical point $r_{\rm out}$ up to infinity, where flow is subsonic. Region II marked with yellow dashed lines corresponds to the flow inside $r_{\rm out}$ and outside $r_{\rm shock}$, where flow is supersonic. Region III marked with green dash-dotted lines corresponds to the flow inside the shock $r_{\rm shock}$ and outside the inner critical point $r_{\rm in}$, where flow is again subsonic. Region IV marked with red dotted lines corresponds to the flow inside the inner critical point $r_{\rm in}$ up to the minimum radius where flow can be extended outside the real Kerr black hole horizon and the flow is supersonic again. All the lines correspond to $r=$ constant lines in their corresponding regions expect for the lines at boundaries where the $r=$ constant lines coincide with $t=$ constant lines where the time values are as specified in the figures.

diagram of adiabatic flow with height as prescribed by Novikov and Thorne and isothermal flows for both the disc heights is that whereas for the former case the sonic points are not the acoustic black hole horizons; for the later set of models, the sonic points and the acoustic black hole horizons are isomorphic. All the conclusions drawn in the case of adiabatic flow for conical disc height are although applicable for isothermal flows with both disc heights as the sonic points are isomorphic with the acoustic black hole horizons for these cases. Thus we restrain ourselves from the repetitive analysis and present the diagrams which are self-explanatory following the discussion of adiabatic flow.

VII. CONCLUDING REMARKS

Accretion flow in hydrostatic equilibrium along the transverse direction differs from flows with other geometrical configurations in that, for flow in hydrostatic equilibrium the critical points do not coincide with the corresponding conventional sonic points. By conventional Mach number, we mean that the associated characteristic speed is assumed to be the stationary sound speed defined by $c_s^2 = \gamma p/\rho$, whereas for acoustic geometry embedded within the accretion flow, the speed of propagation of the linear perturbation is taken to be the dynamical sound speed and is designated as the effective sound speed $c_{\rm eff}$ as defined at the critical point. Such a standalone role (in comparison to the other flow geometries) of the flow in hydrostatic equilibrium is because of the presence of the (stationary) sound speed in the expression of the disc height. The expression for the disc height is obtained by balancing the gravitational force with the pressure force and while doing so, a certain set of idealized assumptions have been made where the derivative of the height function is approximated to the ratio of the local height to the radial distance in Newtonian limit. Such approximation is made since it has not been possible to construct and solve the Euler equation along the vertical direction (in addition to the radial Euler equation as defined and solved along the equatorial plane), and hence the radial sound speed enters in the expression of the disc height. A disc height obtained by such set of approximation is not completely realistic but that is the best one can do for accretion of ideal hydrodynamic fluid. For non ideal non hydrodynamic flow, certain other prescriptions are available which have been obtained by employing the non-LTE radiative transfer method or by using the Grad-Shafranov equations for the magnetohydrodynamics or MHD flow [70–74]. For our purpose, however, we stick to the ideal fluid for the sake of Lorentz invariance.

We have demonstrated that an acoustic white hole forms at the shock location. At the shock location, the dynamical velocity as well as the characteristic sound speed changes discontinuously, and hence their space derivatives diverge. This does not allow us to compute the acoustic surface gravity at the shock location. Acoustic surface gravity at the white hole, thus, diverges. That is primarily because of the fact that the shock has been assumed to have infinitesimally small (practically zero) thickness. Had it been the case that we would consider a shock with finite thickness, the acoustic surface gravity at the acoustic white hole would be extremely large but finite. Possibilities of having such unusually large acoustic surface gravity have been discussed in other contexts. It is to be mentioned that a shock with finite thickness may have different temperature at its two sides, leading to the dissipation of energy at the shock through radiation. Since our analog model requires the fluid to be nondissipative, we are somewhat compelled to consider shock with zero thickness only.

Figure 4 depicts the corresponding Carter-Penrose diagram of isothermal accretion of matter flow in hydrostatic equilibrium along the transverse direction where the disc height is provided by the work of Novikov and Thorne [60]. It is evident from the figure that there is a lack of continuity between the region represented by yellow lines and that by green lines. Such a trend in the causal structure indicates that the region from the outer sonic point to the shock location does not cover the entire manifold of analog spacetime. The shape of the terminal green line representing the shock location proves that the shock is the boundary from which all future directed null sonic trajectories in the region between $r_{\rm out}$ and $r_{\rm sh}$ should escape ultimately to the subsonic region between $r_{\rm sh}$ and $r_{\rm in}$. This establishes the shock to be the white hole with respect to any observer from the aforementioned subsonic region. The problem with this interpretation is that the region just outside the green line representing $r_{\rm sh}$ is not in the manifold, as mentioned. This is the artifact of the situation that the flow becomes discontinuous at the shock. This happens because the kind of shock we consider has zero thickness, i.e., we have not been able to deal with a shock with finite thickness. It is expected that a continuous flow, which is a consequence of the finite width of the shock, will not have the problem of exclusion of a part of the manifold.

For multitransonic shocked flow, accreting matter first encounters the outer sonic point, that is, as if it "disappears" from the "outer acoustic universe" (spacetime spanned from infinity up to the outer sonic point) once it becomes supersonic for the first time. It means that once it crosses the outer acoustic black hole type horizon, i.e., the outer sonic point, no sonic signal emitted by any observer comoving with the matter will be able to reach any other observer situated in between infinity and the outer sonic point (observer comoving with subsonic flow). Once the supersonic matter, however, encounters the shock, the postshock accretion flow resembles matter which has been "thrown out" to "another universe" through the acoustic white hole, i.e., the stationary shock. The overall phenomena is equivalent to disappearance of matter from one universe through a black hole and reappearance of that matter to some

other universe through a white hole. Such acoustic black-hole–white-hole combination, thus acts as a sonic analog of a wormhole. In our next work, we plan to introduce the properties of such acoustic worm holes in detail.

ACKNOWLEDGMENTS

Authors thank the reviewers for useful and constructive comments which helped the authors to improve the manuscript.

[1] J. Fukue, Shock propagations in a geometrically thin accretion disk, Publ. Astron. Soc. Jpn. **35**, 355 (1983).
[2] J. F. Lu, Non-uniqueness of transonic solution for accretion onto a Schwarzschild black hole, Astron. Astrophys. **148**, 176 (1985).
[3] J. F. Lu, Sound horizon of accretion onto a Kerr black hole, Gen. Relativ. Gravit. **18**, 45 (1986).
[4] J. Fukue, Transonic disk accretion revisited, Publ. Astron. Soc. Jpn. **39**, 309 (1987).
[5] K. Nakayama, Dynamical instability of standing shock waves in adiabatic accretion flows and wind flows, Mon. Not. R. Astron. Soc. **270**, 871 (1994).
[6] R. Yang and M. Kafatos, Shock study in fully relativistic isothermal flows, 2, Astron. Astrophys. **295**, 238 (1995).
[7] S. K. Chakrabarti, Global solutions of viscous transonic flows in Kerr geometry—I. Weak viscosity limit, Mon. Not. R. Astron. Soc. **283**, 325 (1996).
[8] V. I. Pariev, Hydrodynamic accretion on to a rapidly rotating Kerr black hole, Mon. Not. R. Astron. Soc. **283**, 1264 (1996).
[9] J. F. Lu, K. N. Yu, F. Yuan, and E. C. M. Young, Standing Rankine-Hugoniot shocks in accretion and wind flows in Kerr geometry, Astron. Astrophys. **321**, 665 (1997).
[10] J. Peitz and S. Appl, Viscous accretion discs around rotating black holes, Mon. Not. R. Astron. Soc. **286**, 681 (1997).
[11] R. Takahashi, Horizon-penetrating transonic accretion discs around rotating black holes, Mon. Not. R. Astron. Soc. **382**, 567 (2007).
[12] P. Barai, T. K. Das, and P. J. Wiita, The dependence of general relativistic accretion on black hole spin, Astrophys. J. Lett. **613**, L49 (2004).
[13] H. Nagakura and S. Yamada, General relativistic hydrodynamic simulations and linear analysis of the standing accretion shock instability around a black hole, Astrophys. J. **689**, 391 (2008).
[14] H. Nagakura and S. Yamada, The standing accretion shock instability in the disk around the Kerr black hole, Astrophys. J. **696**, 2026 (2009).
[15] T. K. Das and B. Czerny, Hysteresis effects and diagnostics of the shock formation in low angular momentum axisymmetric accretion in the Kerr metric, New Astron. **17**, 254 (2012).
[16] T. K. Das, S. Nag, S. Hegde, S. Bhattacharya, I. Maity, B. Czerny, P. Barai, P. J. Wiita, V. Karas, and T. Naskar, Black hole spin dependence of general relativistic multi-transonic accretion close to the horizon, New Astron. **37**, 81 (2015).
[17] P. Tarafdar and T. K. Das, Dependence of acoustic surface gravity on geometric configuration of matter for axially symmetric background flows in the schwarzschild metric, Int. J. Mod. Phys. D **24**, 1550096 (2015).
[18] P. Suková and A. Janiuk, Shocks in the low angular momentum accretion flow, J. Phys. Conf. Ser. **600**, 012012 (2015).
[19] T. Le, K. S. Wood, M. T. Wolff, P. A. Becker, and J. Putney, Standing shock instability in advection-dominated accretion flows, Astrophys. J. **819**, 112 (2016).
[20] P. Suková, S. Charzyński, and A. Janiuk, Shocks in the relativistic transonic accretion with low angular momentum, Mon. Not. R. Astron. Soc. **472**, 4327 (2017).
[21] I. Palit, A. Janiuk, and P. Sukova, Effects of adiabatic index on the sonic surface and time variability of low angular momentum accretion flows, Mon. Not. R. Astron. Soc. **487**, 755 (2019).
[22] I. Palit, A. Janiuk, and P. Sukova, Time variability of low angular momentum accretion flows around black hole, Proc. Sci., HEPROVII (**2020**) 068.
[23] I. Palit, A. Janiuk, and B. Czerny, Clumpy wind accretion in Cygnus x-1, Astrophys. J. **904**, 21 (2020).
[24] P. Tarafdar, S. Maity, and T. K. Das, Influence of flow thickness on general relativistic low angular momentum accretion around spinning black holes, Phys. Rev. D **103**, 023023 (2021).
[25] A. K. Ray and J. K. Bhattacharjee, Realizability of stationary spherically symmetric transonic accretion, Phys. Rev. E **66**, 066303 (2002).
[26] A. K. Ray, Linearized perturbation on stationary inflow solutions in an inviscid and thin accretion disc, Mon. Not. R. Astron. Soc. **344**, 83 (2003).
[27] A. K. Ray, Viscosity in spherically symmetric accretion, Mon. Not. R. Astron. Soc. **344**, 1085 (2003).
[28] A. K. Ray and J. K. Bhattacharjee, A dynamical systems approach to a thin accretion disc and its time-dependent behaviour on large length scales (2005).
[29] A. K. Ray and J. K. Bhattacharjee, Large-scale properties in turbulent spherically symmetric accretion, Astrophys. J. **627**, 368 (2005).
[30] A. K. Ray and J. K. Bhattacharjee, Evolution of transonicity in an accretion disc, Classical Quantum Gravity **24**, 1479 (2007).
[31] J. K. Bhattacharjee and A. K. Ray, Secular instability in quasi-viscous disk accretion, Astrophys. J. **668**, 409 (2007).
[32] J. K. Bhattacharjee, A. Bhattacharya, T. K. Das, and A. K. Ray, Quasi-viscous accretion flow—I. Equilibrium conditions and asymptotic behaviour, Mon. Not. R. Astron. Soc. **398**, 841 (2009).
[33] S. Chaudhury, A. K. Ray, and T. K. Das, Critical properties and stability of stationary solutions in multitransonic

pseudo-Schwarzschild accretion, Mon. Not. R. Astron. Soc. **373**, 146 (2006).
[34] I. Mandal, A. K. Ray, and T. K. Das, Critical properties of spherically symmetric black hole accretion in Schwarzschild geometry, Mon. Not. R. Astron. Soc. **378**, 1400 (2007).
[35] S. Goswami, S. N. Khan, A. K. Ray, and T. K. Das, Axisymmetric black hole accretion in the Kerr metric as an autonomous dynamical system, Mon. Not. R. Astron. Soc. **378**, 1407 (2007).
[36] S. K. Chakrabarti and S. Das, Model dependence of transonic properties of accretion flows around black holes, Mon. Not. R. Astron. Soc. **327**, 808 (2001).
[37] N. Bilic, A. Choudhary, T. K. Das, and S. Nag, The role of axisymmetric flow configuration in the estimation of the analogue surface gravity and related Hawking-like temperature, Classical Quantum Gravity **31**, 035002 (2014).
[38] L. C. Ho, Supermassive black holes in galactic nuclei, in *Observational Evidence for Black Holes in the Universe*, edited by S. K. Chakrabarti (Springer, Netherlands, Dordrecht, 1999), pp. 157–186.
[39] I. V. Igumenshchev and M. A. Abramowicz, Rotating accretion flows around black holes: Convection and variability, Mon. Not. R. Astron. Soc. **303**, 309 (1999).
[40] V. Moncrief, Stability of stationary, spherical accretion onto a Schwarzschild black hole, Astrophys. J. **235**, 1038 (1980).
[41] W. G. Unruh, Experimental Black-Hole Evaporation?, Phys. Rev. Lett. **46**, 1351 (1981).
[42] M. Visser, Acoustic black holes: Horizons, ergospheres and hawking radiation, Classical Quantum Gravity **15**, 1767 (1998).
[43] C. Barcelo, S. Liberati, and M. Visser, Analogue gravity, Living Rev. Relativity **8**, 12 (2005).
[44] T. K. Das, Analogue Hawking radiation from astrophysical black-hole accretion, Classical Quantum Gravity **21**, 5253 (2004).
[45] S. Dasgupta, N. Bilic, and T. K. Das, Pseudo-schwarzschild spherical accretion as a classical black hole analogue, Gen. Relativ. Gravit. **37**, 1877 (2005).
[46] H. Abraham, N. Bilic, and T. K. Das, Acoustic horizons in axially symmetric relativistic accretion, Classical Quantum Gravity **23**, 2371 (2006).
[47] T. K. Das, N. Bilić, and S. Dasgupta, A black-hole accretion disc as an analogue gravity model, J. Cosmol. Astropart. Phys. 06 (2007) 009.
[48] H.-Y. Pu, I. Maity, T. K. Das, and H.-K. Chang, On spin dependence of relativistic acoustic geometry, Classical Quantum Gravity **29**, 245020 (2012).
[49] S. Saha, S. Sen, S. Nag, S. Raychowdhury, and T. K. Das, Model dependence of the multi-transonic behaviour, stability properties and the corresponding acoustic geometry for accretion onto rotating black holes, New Astron. **43**, 10 (2016).
[50] M. A. Shaikh, I. Firdousi, and T. K. Das, Relativistic sonic geometry for isothermal accretion in the Schwarzschild metric, Classical Quantum Gravity **34**, 155008 (2017).
[51] P. Tarafdar and T. K. Das, Influence of the geometric configuration of accretion flow on the black hole spin dependence of relativistic acoustic geometry, Int. J. Mod. Phys. D **27**, 1850023 (2018).
[52] M. A. Shaikh, Relativistic sonic geometry for isothermal accretion in the Kerr metric, Classical Quantum Gravity **35**, 055002 (2018).
[53] M. A. Shaikh and T. K. Das, Linear perturbations of low angular momentum accretion flow in the Kerr metric and the corresponding emergent gravity phenomena, Phys. Rev. D **98**, 123022 (2018).
[54] M. A. Shaikh, S. Maity, S. Nag, and T. K. Das, Effective sound speed in relativistic accretion discs around Schwarzschild black holes, New Astron. **69**, 48 (2019).
[55] B. Carter, Complete analytic extension of the symmetry axis of Kerr's solution of Einstein's equations, Phys. Rev. **141**, 1242 (1966).
[56] R. Penrose, Republication of: Conformal treatment of infinity, Gen. Relativ. Gravit. **43**, 901 (2011).
[57] B. Carter, Global structure of the Kerr family of gravitational fields, Phys. Rev. **174**, 1559 (1968).
[58] R. H. Boyer and R. W. Lindquist, Maximal analytic extension of the Kerr metric, J. Math. Phys. (N.Y.) **8**, 265 (1967).
[59] M. Walker, Block diagrams and the extension of timelike two surfaces, J. Math. Phys. (N.Y.) **11**, 2280 (1970).
[60] I. D. Novikov and K. S. Thorne, Astrophysics of black holes, in *Black Holes (Les Astres Occlus)*, edited by C. Dewitt and B. S. Dewitt (Gordon and Breach Science Publishers, Inc., New York, NY, 1973), pp. 343–450.
[61] H. Riffert and H. Herold, Relativistic accretion disk structure revisited, Astrophys. J. **450**, 508 (1995).
[62] P. Tarafdar, D. A. Bollimpalli, S. Nag, and T. K. Das, Influence of geometrical configuration on low angular momentum relativistic accretion around rotating black holes, Phys. Rev. D **100**, 043024 (2019).
[63] C. F. Gammie and R. Popham, Advection-dominated accretion flows in the Kerr metric. I. Basic equations, Astrophys. J. **498**, 313 (1998).
[64] M. A. Abramowicz, A. Lanza, and M. J. Percival, Accretion disks around Kerr black holes: Vertical equilibrium revisited, Astrophys. J. **479**, 179 (1997).
[65] D. B. Ananda, S. Bhattacharya, and T. K. Das, Acoustic geometry through perturbation of mass accretion rate: Radial flow in static spacetimes, Gen. Relativ. Gravit. **47**, 96 (2015).
[66] D. A. Bollimpalli, S. Bhattacharya, and T. K. Das, Perturbation of mass accretion rate, associated acoustic geometry and stability analysis, New Astron. **51**, 153 (2017).
[67] R. M. Wald, *General Relativity* (Chicago University Press, Chicago, IL, 1984).
[68] P. G. Frè, *Gravity, a Geometrical Course, Volume 2: Black Holes, Cosmology and Introduction to Supergravity* (Springer, Dordrecht, 2013).
[69] C. Barceló, S. Liberati, S. Sonego, and M. Visser, Causal structure of analogue spacetimes, New J. Phys. **6**, 186 (2004).
[70] I. Hubeny and V. Hubeny, Non-LTE models and theoretical spectra of accretion disks in active galactic nuclei. II. Vertical structure of the disk, Astrophys. J. **505**, 558 (1998).

[71] S. W. Davis and I. Hubeny, A grid of relativistic, non-LTE accretion disk models for spectral fitting of black hole binaries, Astrophys. J. Suppl. Ser. **164**, 530 (2006).

[72] V. S. Beskin, Reviews of topical problems: Axisymmetric stationary flows in compact astrophysical objects, Phys. Usp. **40**, 659 (1997).

[73] V. Beskin and A. Tchekhovskoy, Two-dimensional structure of thin transonic discs: Theory and observational manifestations, Astron. Astrophys. **433**, 619 (2005).

[74] V. S. Beskin, *MHD Flows in Compact Astrophysical Objects: Accretion, Winds and Jets*, Astronomy and Astrophysics Library (Springer-Verlag, Berlin Heidelberg, 2010).